NUMERICAL SIMULATION OF FLUID DYNAMICS IN TWO LITERS BIOREACTOR AND ITS SCALE-UP APPLICATIONS

MR. PISUT VEERAHONG

A SPECIAL RESEARCH PROJECT SUBMITTED IN PARTIAL FULFILLMENT
OF THE REQUIREMENTS FOR
THE DEGREE OF MASTER OF ENGINEERING (CHEMICAL ENGINEERING)
FACULTY OF ENGINEERING
KING MONGKUT'S UNIVERSITY OF TECHNOLOGY THONBURI
2011

Numerical Simulation of Fluid Dynamics in Two Liters Bioreactor and Its Scale-Up Applications

Mr. Pisut Veerahong B.Eng. (Chemical Engineering)

A Special Research Project Submitted in Partial Fulfillment
of the Requirements for
the Degree of Master of Engineering (Chemical Engineering)
Faculty of Engineering
King Mongkut's University of Technology Thonburi
2011

Special Research Project Committee

..... (Asst. Prof. Anan Tongta, Ph.D.)	Chairman
..... (Lect. Panit Kitsubun, Ph.D.)	Member and Special Research Project Advisor
..... (Asst. Prof. Jindarat Pimsamarn, Ph.D.)	Member and Special Research Project Co-Advisor
..... (Lect. Wimolsiri Pridasawas, Ph.D.)	Member
..... (Pornkamol Unrean, Ph.D.)	Member

Special Research Project Title	Numerical Simulation of Fluid Dynamics in Two Liters Bioreactor and Its Scale-Up Applications
Special Research Project Credits	6
Candidate	Mr. Pisut Veerahong
Special Research Project Advisor	Dr. Panit Kitsubun
Special Research Project Co-Advisor	Asst. Prof. Dr. Jindarat Pimsamarn
Program	Master of Engineering
Field of Study	Chemical Engineering
Department	Chemical Engineering
Faculty	Engineering
B.E.	2554

Abstract

The computational fluid dynamics coupled with population balance method was used to investigate the hydrodynamics and mass transfer in a 2 L bioreactor. A population balance model was used in order to account for the effect of bubble breakup and coalescence in the bioreactor. Multiple frame of reference method was used to model the rotating regions. The local hydrodynamics predicted from CFD model such as gas holdup, Sauter mean bubble diameter, turbulence energy dissipation rate and dissolved oxygen were investigated. The local mass transfer coefficient (k_La) was calculated using Higbie's penetration theory and Eddy cell model. The overall mass transfer coefficients predicted by the CFD model were compared with the experimental measurements. The experiments to determine the overall mass transfer coefficient were performed using gassing out technique. From the results, the predicted mass transfer coefficient from eddy cell model matches very well with the experimental result while the predicted mass transfer coefficient from Higbie's penetration theory gives higher value compared to the experimental result. After the CFD model of 2 L bioreactor was successfully developed, the scale-up of the bioreactor from 2 L scale to 200 L scale was performed based on constant mass transfer coefficient criteria. The model of 200 L bioreactor was developed using the same technique with 2 L bioreactor. In maintaining a constant k_La upon scale-up from 2 to 200 liter, the agitation speed and the air inlet flowrate could not be maintained, adjustment has to be done. The scale-up equation based on constant power consumption per unit liquid volume and impeller tip speed was used in order to determine the operating agitation speed of 200 L bioreactor. Air feed rate was varied in order to obtain the similar k_La value. From the results, scale-up procedure based on constant k_La criteria was successfully employed in this study. The operating variables at 200 liter bioreactor scale were achieved.

Keywords: Bioreactor / CFD / Mass transfer coefficient / Scale-up

หัวข้อโครงการศึกษาวิจัย	การสร้างแบบจำลองสภาวะการไหลในถังปฏิกรณ์ชีวภาพขนาด 2 ลิตร และการนำไปประยุกต์ใช้ในการขยายขนาดของถังปฏิกรณ์ชีวภาพ
หน่วยกิต	6
ผู้เขียน	นายพิศุทธิ์ วีระหงษ์
อาจารย์ที่ปรึกษา	ดร.พนิต กิจสุบรรณ
อาจารย์ที่ปรึกษาร่วม	ผศ.ดร.จินดารัตน์ พิมพ์สมาน
หลักสูตร	วิศวกรรมศาสตรมหาบัณฑิต
สาขาวิชา	วิศวกรรมเคมี
ภาควิชา	วิศวกรรมเคมี
คณะ	วิศวกรรมศาสตร์
พ.ศ.	2554

บทคัดย่อ

งานวิจัยชิ้นนี้ได้ทำการศึกษาพฤติกรรมทางด้านอุทกพลศาสตร์และการถ่ายเทมวลที่เกิดขึ้นภายในถังปฏิกรณ์ชีวภาพขนาด 2 ลิตร โดยใช้แบบจำลองพลศาสตร์การไหลด้วยวิธีทางคอมพิวเตอร์ร่วมกับทฤษฎี Population balance โดยที่ทฤษฎี Population balance เป็นทฤษฎีที่นำมาใช้เพื่อศึกษาผลกระทบของการแตกตัวและรวมตัวของฟองก๊าซที่เกิดขึ้นภายในถังปฏิกรณ์ชีวภาพ การจำลองการหมุนของใบกวนในงานวิจัยนี้ใช้วิธีจำลองการไหลแบบ Multiple Frame of Reference โดยตัวแปรด้านอุทกพลศาสตร์ที่ทำการศึกษาได้แก่ ค่าสัดส่วนของก๊าซรวมภายในระบบ เส้นผ่านศูนย์กลางเฉลี่ยของฟองก๊าซแบบซอเทอร์ อัตราการลดลงของพลังงานจลน์ของความปั่นป่วนและปริมาณการละลายของออกซิเจน การทดลองเพื่อหาค่าการถ่ายเทมวลสารโดยรวมระหว่างวัฏภาคก๊าซและของเหลวกระทำการทดลองโดยวิธี gassing out ค่าสัมประสิทธิ์การถ่ายเทมวลสารโดยรวมระหว่างวัฏภาคก๊าซและของเหลวที่คำนวณได้จากทฤษฎี Higbie’s penetration และ Eddy cell จะถูกนำมาเปรียบเทียบกับค่าสัมประสิทธิ์การถ่ายเทมวลสารโดยรวมระหว่างวัฏภาคก๊าซและของเหลวที่ได้จากการทดลองเพื่อตรวจสอบความถูกต้องของแบบจำลองทางพลศาสตร์ที่สร้างขึ้น จากผลการทดลองพบว่าค่าสัมประสิทธิ์การถ่ายเทมวลสารโดยรวมระหว่างวัฏภาคก๊าซและของเหลวที่คำนวณได้จากทฤษฎี Eddy cell มีค่าที่ใกล้เคียงกับผลการทดลอง ส่วนค่าที่คำนวณได้จากทฤษฎี Higbie’s penetration มีค่าสูงกว่าค่าที่ได้จากผลการทดลอง งานวิจัยนี้ยังได้ทำการศึกษาการขยายขนาดของถังปฏิกรณ์ชีวภาพจากขนาด 2 ลิตรไปยังขนาด 200 ลิตร โดยให้ค่าสัมประสิทธิ์การถ่ายเทมวลมีค่าคงที่ โดยปกติแล้วในการขยายขนาดถังปฏิกรณ์ชีวภาพ ค่าความเร็วรอบในการกวนและอัตราการให้อากาศของถังปฏิกรณ์ชีวภาพขนาดเล็กจะไม่สามารถนำไปใช้กับถังปฏิกรณ์ชีวภาพขนาดใหญ่ได้ ดังนั้นใน

งานวิจัยนี้ได้ใช้สมการการขยายขนาดเพื่อหาค่าความเร็วรอบการกวนของถังปฏิกรณ์ขนาด 200 ลิตร และทำการปรับเปลี่ยนอัตราการป้อนอากาศเพื่อให้ได้ค่าสัมประสิทธิ์การถ่ายเทมวลเท่ากับถังปฏิกรณ์ของ 2 ลิตร จากผลการทดลองจะเห็นว่างานวิจัยนี้ประสบผลสำเร็จในการขยายขนาดของถังปฏิกรณ์ชีวภาพ ค่าสัมประสิทธิ์การถ่ายเทมวลที่ได้จากแบบจำลองของถังปฏิกรณ์ชีวภาพขนาด 200 ลิตรค่าใกล้เคียงกับค่าที่ได้จากแบบจำลองของถังปฏิกรณ์ชีวภาพขนาด 2 ลิตร

คำสำคัญ : การขยายขนาด / ค่าสัมประสิทธิ์การถ่ายเทมวล / ถังปฏิกรณ์ชีวภาพ / แบบจำลองพลศาสตร์การไหล

ACKNOWLEDGEMENTS

I would like to express my gratitude to these people who help me through the course of study. Firstly, I would like to express my appreciation to my project advisor, Dr. Panit Kitsubun and my project co-advisor, Asst. Prof. Jindarat Pimsamarn for their support, valuable comments and valuable suggestions. Next, I would like to thank Asst. Prof. Anan Tongta, Dr. Wimolsiri Pridasawas and Dr. Pornkamol Unrean, members of my thesis committee, for giving valuable ideas to improve my work.

Moreover, my appreciation also goes to my friends in ChEPS class 14 who are friendly, sincerely and caring. I would like to extend special thanks the ChEPS program that provided me a lot of good experience. Last but not least, I would like to especially thank my family for their supports, encouragement and warm understanding.

CONTENTS

LIST OF TABLES

TABLE **PAGE**

LIST OF FIGURES

FIGURE **PAGE**

LIST OF TECHNICAL SYMBOLS AND ABBREVIATIONS

a	=	gas-liquid interface area per liquid volume (cm^2/cm^3)
C_L	=	Concentration of dissolved oxygen ($mmoles/dm^3$)
C^*	=	Saturated dissolves oxygen concentration ($mmoles/dm^3$)
c_μ	=	turbulence model constant depending on the model used
D	=	Diffusion coefficient (m^2/s)
D_i	=	Impeller diameter (m)
D_T	=	Tank Diameter (m)
H_T	=	Liquid Height (m)
k_L	=	Local mass transfer coefficient (m/s)
k_La	=	Overall mass transfer coefficient (s^{-1})
m	=	Constant in Michel and Miller's equation
N	=	Impeller speed (rpm)
N_P	=	Power number
P_0	=	Power in ungassed system (w)
P_g	=	Gassed power consumption (w)
Q	=	Air flow rate (m^3/s)
r_α	=	volume fraction of phase α
v_g	=	Superficial air velocity (m/s)
V_L	=	Liquid Volume (m^3)
S_α	=	Source term (kg/m^3s)
k	=	turbulent kinetic energy (m^2/s^2)
ρ_α	=	phase density (kg/m^3)
μ	=	molecular (dynamics) viscosity (kg/ms)
μ_{tl}	=	liquid phase turbulence viscosity (kg/ms)
ε	=	the turbulent dissipation rate (m^2/s^3)

CHAPTER 1 INTRODUCTION

1.1 Background

Mechanically agitated aerobic fermenters are widely used in biotechnology, food, and pharmaceutical industries. Understanding and modeling the complex interactions between biological reaction and hydrodynamics are a key problem when dealing with bioprocesses. For a better operation, the hydrodynamics of flows in bioreactor must be understood. Many experimental studies have been made over the years to investigate fluid flow in bioreactor. However, the application of the experimental techniques used to investigate flow fields, heat fluxes, and mass concentration fields are extremely costly and highly limited in application [1]. Most available models are limited to a specific scale and operating conditions. Therefore, it is essential to develop and apply new tools to enhance our understanding of hydrodynamic and highly complex fluid flow of stirred bioreactors. Computational fluid dynamics (CFD) has clearly emerged as a promising tool for the simulation of local hydrodynamics in aerated stirred bioreactor [2]. Modern CFD software can predict fluid flow, heat and mass transfer and can improve the knowledge of information about turbulent flow field, gas hold up, interfacial area and bubble size.

Bioreactors have the potential to produce high value products and replace of existing chemical-based commodity processes. Stirred tank bioreactors with baffles and agitators are commonly used in fermentation process, which have the dual advantages of low capital and operating costs. A stirred tank is an often used contactor, mainly as a reactor, in which gas or mixture of gases is distributed in form of bubbles in the liquid, by an appropriate distributor and an agitation system. Tanks are fitted with baffles, which prevent a large central vortex being formed as well as improve mixing. Four baffles are used for vessels less than 3 meters in diameter, and six to eight baffles are used in larger vessels. The fractional gas hold up in the stirred tank reactor is a basic measurement of the efficiency of gas liquid contacting.

In fermentation processes, all microorganisms require nutrients for propagation and to produce metabolites as useful by-products. Nutrients are frequently added into media in excessive amounts than are required by the cell, but the amounts of trace metals and minerals supplied are limited [3]. For aerobic fermentation, oxygen is required as an essential nutrient. It needs special attention on both the consumption by microorganisms and supply capacity of bioreactors. The presence of salts and other nutrients required for the growth of any organism can reduce the solubility of oxygen [4]. The main problem with oxygen comes from its low solubility in aqueous phase. Therefore, the major challenge in aerobic fermentation is an increase of oxygen mass transfer rate**.**

Oxygen transfer through microbial cells controls the most of aerated biological system [5]. The amount of dissolved oxygen into broth is limited by its solubility, mass transfer rate and its consumption rate of microbial cells. The rate of oxygen transfer to the cell is one of the limiting factors in product formation. It is known that increasing the rate of oxygen transfer can enhance the rate of product formation [6]. Moreover, Oxygen transfer of an industrial fermentation process is a function of aeration and agitation. The agitation rate of the fermenter affects the coalescence and breakup of bubbles, bubble size distribution, and bubble residence time. For large-scale systems, power consumption during aeration and agitation is a significant fraction of the total operating cost. To increase agitation rate, the power of the impeller motor must be increased.

However, there are limits to the speed of agitation. The increase in agitation rate produces higher shear stress in the broth, which may cause a decrease in the growth of shear-sensitive microorganisms [5].

Mass transfer effectiveness is most frequently assessed in gas-liquid contactors by measuring the volumetric mass transfer coefficient, k_La. Gas-liquid mass transfer is commonly the rate-limiting step in industrial-scale biochemical. For this reason, bioreactor design and scale-up providing ample gas mass transfer. During the scale-up aerobic bioprocess, in aerated stirred tank, maintaining a constant volumetric mass transfer coefficient is the most commonly used criterion. Several models have been proposed in the literature for determining the k_L. Most of the models proposed are based on the concept of a rigid interface or surface renewal. The classical model which is based on the concept of rigid interface is the two-film model. The model which is based on the concept of surface renewal is Higbie penetration model.

Over the years many experimental studies have been made to investigate the characteristics of gas dispersion in stirred tank as it influences the mass transfer effectiveness. These studies usually result in empirical correlations for overall quantities such as power consumption, gas holdup, and mixing times. These correlations cannot usually reflect the details of the physics involved in mass transfer and will only apply to the narrow range of experimental conditions for which they have been determined [7]. During the last two decades, computational fluid dynamics (CFD) techniques have been used to calculate fluid flow in agitated tanks by several researchers. With computational fluid dynamics (CFD), it is possible to model local conditions in arbitrary vessel geometries.

The modeling situation is complex when multiphase flows are involved. Transport equations for mass, momentum, and turbulence properties have to be solved for each individual phase. A few researchers have attempted to study process characteristics in an aerated tank using CFD methods, and some progress has been made in recent years [8]. In literature, an Eulerian multi-fluid based model has been successfully used to study the gas dispersion in stirred tank reactor without incorporating the bubble size distributions [7]. A constant bubble size is assumed. However, the most important issue in gas-liquid dispersion modeling is the prediction of bubble size and gas-liquid interfacial area. The prediction of bubble size distribution is required when the model accuracy is needed. The bubble size distribution is important since the interfacial area is the key parameter that controls the oxygen transfer rate. Prediction of bubble size distribution was carried by many researches using the population balance equation for turbulence gas dispersion in tank. The population balance is written considering bubble break up and coalescence processes.

Widely used population balance models are based on bubble number density (BND), quadrature method of moments (QMOM) and multiple size group model (MUSIG). BND model is simple and is basically calculated from gas phase volume fraction by solving scalar type of transport equation and it requires less computational cost. In Quadrature method of moments, the equations are solved for the moments of the bubble size distributions using quadrature approximation and this method also requires more or less computational cost compared to the full population balance equations. The MUSIG model of population balance equations assumes that the bubbles of varying size have

the same velocity [9]. Several researches have studied the hydrodynamics and mass transfer in bioreactor using coupling CFD and population balance models.

This research used Computational Fluid Dynamics software package to study the flow behavior and oxygen transfer in bioreactors cell fermentation. ANSYS CFX, the commercial CFD code is used to predict of hydrodynamics parameters, gas holdup, local bubble-size distributions and mass transfer coefficient. Subsequently, the scale-up studies based on the constant oxygen transfer coefficient, k_La from 2L to 200L of aerated and agitated bioreactor were performed. Moreover, concentration of dissolved oxygen was monitored as scalars, which can hence be solved using transport equation. Eulerian multiphase and population balance equation-multiple size group (MUSIG) models have been implemented. With knowledge of the local bubble size, the local oxygen transfer coefficient in the tanks was estimated using the Higbie's penetration theory and eddy cell model.

Additionally, the scale-up of a bioprocess from lab-scale to industrial scale often results in a decrease of the productivity compared to the lab-scale ones. Success of scale-up from laboratory scale to manufacturing scale in process development requires understanding of local hydrodynamics in bioreactor at different scale [10]. Fermenters operating at different scales cannot be operated in the same environmental conditions and the scale-up based on a single engineering parameter is not possible because of the relative change in other parameters. In order to address the scale-up problems robustly it is important to identify the critical process. Once the critical parameters are identified the scale-up strategies based on critical parameters can be proposed [11]. Normally, the critical parameter in fermentation process is oxygen transfer coefficient. Maintaining a constant volumetric mass transfer coefficient is a common scale-up strategy for bioprocesses.

1.2 Objectives

The objectives of this research project are:

1. Develop the model of 2L and 200L bioreactor using the CFD technique.
2. Using CFD technique to scale up bioreactor from 2L to 200L based on maintaining a constant volumetric oxygen transfer coefficient criterion.
3. To study the flow behavior and gas-liquid mass transfer inside bioreactor.

1.3 Scopes of work

In order to achieve these objectives, the following scope of work shall be covered:

1. Model of a 2L aerated stirred bioreactor is developed by using commercial CFD package ANSYS CFX version 13. The geometry model of the bioreactor and its mesh were created using ICEM CFD, a mesh-generator software package. The rotating zone was described with a rotating coordinate system using the MRF method.
2. The experiment to determine the overall mass transfer coefficient of chemostat *P.pastoris* medium-air system is performed using Non-fermentative method (Dynamic gassing-out). The predicted overall mass transfer coefficient was compared with the experimental results.
3. Simulation of a two phase flow of 200L bioreactor was performed in the last step. The scale-up studies based on the constant oxygen transfer coefficient, k_La was used.

1.4 Expected result

This thesis aims to deliver a better understanding of the hydrodynamics, fluid flow, and the distribution of oxygen inside the bioreactor which can be very useful for the improvement of fermentation processes.

CHAPTER 2 LITERATURE REVIEW AND THEORY

2.1 Literature Review

Computational fluid dynamics has now become a powerful tool for prediction of gas-liquid flow behavior in stirred tank during the past few decades [12]. Several recent publications have used CFD for investigating hydrodynamics and transport characteristics in aerated stirred tank. Most of the studies are based on two fluid flows model, generally using an Euler-Euler approach with only constant bubble size in order to predict gas-holdup and flow pattern.

Application of CFD on aerated stirred tank using a constant bubble size was studied by several researchers. The simulations of liquid homogenisation were performed by M. Jahoda et al. for a two phase gas–liquid stirred tank using commercial CFD code FLUENT 6.3 numerical software [12]. Experiments were carried out in an aerated agitated charge in a standard tank equipped with 4 baffles and rotational axial impeller using the Reynolds averaged Navier–Stokes method with the k–ε mixture (MKE) turbulence model. Both the multiple reference frames (MRF) technique and the sliding mesh (SM) were used for simulation of the impeller motion. The effective bubble size of 4 mm was used for all simulations. Volumetric gas flow rate varied from 1 L/min to 7.5 L/min. A constant gas velocity at gas sparger was determined. The flow in the tank was presumed as an isothermal process; therefore no energy equation was solved. Mass transfer between phases and chemical reactions were neglected. The result shows that the result from simulation of both technique exhibits a good agreement with the experimental data. The SM technique is more accurate, but it is also much more time consuming than the MRF approach. The total simulation time of SM and MRF technique is 27.2 days and 3.2 days respectively. The simulation time of MRF technique is less than the simulation time of SM technique, because there is no mesh motion at the beginning of each time step.

Next, CFD simulation of gluconic acid production in a stirred gas-liquid fermenter was performed by M. Elqotbi et al [6]. The simulation analysis was focused on bioproduction of gluconic acid by Aspergilus niger in a stirred gas liquid fermenter. The configuration using in this study was chosen to be close on the conditions in conventional industrial vessels. Constant bubble size and global gas-liquid mass transfer were assumed. The Euler-Euler “two-fluid” model was used. The results from simulation show good qualitative agreement with the laboratory results. The predicted dissolve oxygen concentration profiles from CFD simulation match very well with experimental results. Moreover, the velocity fields, the local substrate, product and biomass concentration profiles were obtained.

In summary, for gas-liquid stirred tank, most of reports have made assumption that gas bubble has the same size and shape. However, accurate modeling of gas liquid stirred tank requires a population balance model due to presence of strong bubble-liquid interactions. A population balance equation is used to describe the evolution of bubble sizes in two-phase flow. The model is able to predict the bubble size distribution in bubble columns and aerated stirred tank. The distribution of bubble size varies inside the stirred tank depending on the spatial position. Generally, bubble sizes around the impeller discharge are smallest due to breakage caused by high turbulence dissipation rates [13]. Further, the bubble diameter can vary depending on the operating conditions such as superficial gas velocity and pressure, the physical properties such as density,

viscosity and surface tension of liquid phase and the details of sparging device such as free area, hole diameter etc. The bubble size directly affects the interfacial area available for gas-liquid mass transfer. A combined CFD–PBM (population balance modeling) model for aerated stirred tank is a better approach than a two-fluid model with constant bubble size. Prediction of local bubble size and local gas holdup was carried by several researchers using population balance equation.

CFD simulation coupled with population balance equations for aerated stirred tank bioreactors was studied by Hu Zhang et al [10]. In this work, a study of local hydrodynamics in 20 L stirred bioreactor for cultivation of Mammalian cells was carried out with CFD code ANSYS-CFX. The flow patterns, energy dissipation rates, gas volume fraction, gas bubble size distribution and local mass transfer coefficient were displayed throughout the whole bioreactor. Gas liquid flow in bioreactor with multiple impellers is modeled using Eulerlian multi-phase model combined with population balance equation. The flow domain is divided into two symmetric parts (each encompassing two baffles and three impeller blades) and only one part is chosen for the present solution domain in order to save calculation time. A source term at the gas sparger for gas volume fraction and momentum equations is employed and a degassing boundary condition at the top surface is used to account for the gas removal from the reactor. The rotational speed for the impeller and air flow rate were added to the simulator. The result show that the geometry of the impellers, clearance from the bottom, clearance above the upper impeller, impeller spacing and sparging conditions affect the flow patterns in the aerated fermenter. The energy dissipation around the top and the bottom impellers decreases rapidly along radial direction while around the middle impeller the energy dissipation is very high along the impeller pumping jet to the reactor wall. The EDR value up to 10,000 W/kg can be found in most part. Shear damage is dependent on the local maximum energy dissipation rates which can cause damage to mammalian cells. However, from the experimental results, *P. patoris* cells are able to resist quite high value of EDR up to 10,000 W/kg. The gas volume fraction profile shows that the high gas volume fraction regions are found around the shaft. The vertical profile of gas bubble shows that the smallest bubbles are found around three impellers due to break up in highly turbulent intensity. Where the turbulent intensity is low, bubbles become larger due to coalescence. Lastly, the calculated mass transfer coefficient based on Higbie's penetration model agreed well with the experimental data.

The oxygen transfer in tank using a combined CFD and population balance model was investigated [13]. In this work, gas-liquid stirred tank agitated by Rushton turbine and CD-6 impeller was simulated with the FLUENT software. The multiphase simulations were modeled using an Eulerian-Eulerian two-fluid model and the drag coefficient of spherical and distorted bubbles was modeled using the Ishii-Zuber equations. The drag model of Ishii and Zuber was selected because bubbles have a tendency to form a non-spherical shape for diameter greater than about 3 mm. The local bubble size distribution was obtained by solving the PBM. Having obtained the local bubble size, the Higbie's penetration theory was used to estimate local oxygen mass transfer coefficient. The transport equation for dissolved oxygen mass fraction was also solved as a user-defined scalar implemented as a user-defined subroutine. The results show that the predicted gas-liquid hydrodynamics and local bubble sizes were in good agreement with experimental measurements. Moreover, it was observed that the gas dispersion in a larger scale tank was more inhomogeneous and has a lower k_La in comparison to the smaller tanks.

Application of CFD on the prediction of mass transfer in gas-liquid stirred tank was studied by Ranganathan et al [9]. The main aim of this work is to validate the hydrodynamics and mass transfer characteristics in a stirred reactor. In this work, ANSYS CFX-11 was use to simulate the hydrodynamics behavior of gas-liquid flows in a dual Rushton turbine stirred reactor. The population balance including break up and coalescence effect was used to calculate the changing size distribution of dispersed phase. The predicted bubble size and mass transfer parameter were compared with the experimental data. The predicted local mass transfer was obtained from CFD simulation using various models such as penetration, slip velocity, eddy cell and rigid models. For population balance model, the polydispersed gas phase was divided into 21 size groups ranging from 0.1 to 10 mm. From the results, the simulated local sauter mean bubble diameter was in good agreement with the experimental results. The local sauter mean bubble diameter is about 1mm at impeller region where the highest turbulent energy dissipation rate occurs. The mean bubble diameter increases in the region away from the impellers, where the turbulent energy dissipation rate decreases. For the predicted local mass transfer, the k_L obtained from penetration theory model is higher than the experimental. The prediction of k_L is lower for the rigid model as compared to the experimental result. The mass transfer coefficient based on slip velocity and eddy cell model match very well with experimental results.

CFD is also used to study the scale up of an aerated stirred bioreactor. Various chemical engineering scale-up criteria are available in the literature. The scale-up criteria are constant specific power input (P_g/V_L), constant k_La, constant tip speed of the agitator and constant dissolved oxygen concentration. In the scale up of bioreactors, the most commonly a used criterion is maintain a constant oxygen mass transfer value (k_La). The scale-up of gas-liquid stirred tanks is a very challenging task because it is very difficult to maintain a similar mass transfer level from a small vessel to the bigger vessels [13].

Flow patterns generated in vessel stirred by double Rushton impellers were investigated by Rutherford *et al*., using flow visualization and laser dropper anemometry (LDA) technique [14]. The experiments were performed with three different impeller positions. The results show stirred vessel with dual Rushton turbine generate three different stable flow patterns depend on impeller clearance between lower impeller and tank bottom, spacing between two impellers. These flow patterns are defined as parallel, merging and diverging flow pattern depending on the characteristic of the liquid circulation loops, as shown in figure 1. The first pattern was called parallel flow. In this pattern, each impeller produce upper and lower ring vortex leading to the formation of four stable ring vortices. The parallel flow was observed with C1gretaer than 0.2T and C2 greater than 0.385T. C3 value must be less than 0.45T in order to generate this flow pattern. T is tank diameter. The second pattern was called merging flow. The impeller streams merge at an elevation midway between impeller to form two large ring vortices. The impeller clearance and spacing between impeller in this case were set equal to T/3. From experimental results, C1 value must be greater than 0.17T and C2 must be greater than 0.358T in order to maintain this flow pattern. The third flow pattern was called diverging flow. In this flow pattern, the upper impeller produced two ring vortices above and below the impeller disk and the lower Rushton turbine produced one large ring vortex. The diverging flow was observed with C1 equal to 0.15 T, C2 equal to 0.5T and C3 equal to 0.35T.

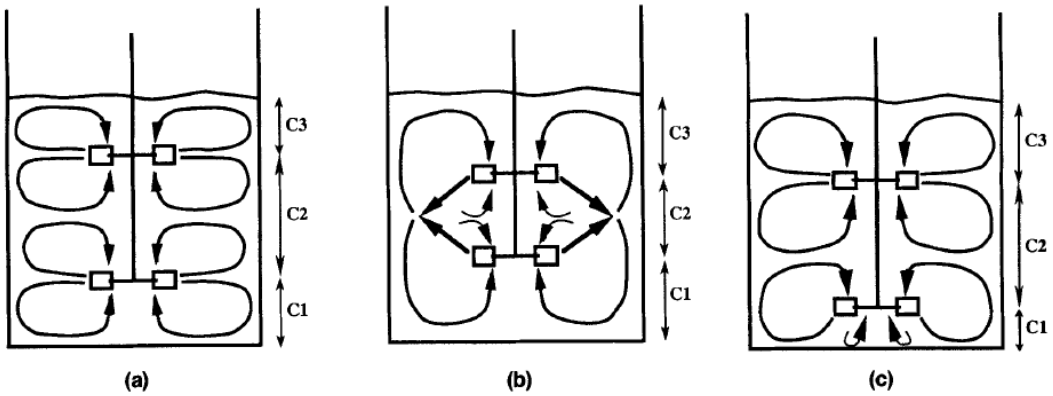

Figure 2.1 Flow patterns of three flow configurations obtained in dual Rushton turbine stirred vessel (a) Parallel flow (b) merging flow (c) diverging flow

2.2 Introduction to Computational Fluid Dynamics (CFD)

Computational Fluid Dynamics (CFD) is a computer-based tool for simulating the behavior of systems involving fluid flow, heat transfer, and other related physical processes. The concept of CFD is to utilize the computer in the numerical calculation of a complex mathematical model. The differential equations of motion are transformed to a large number of algebraic equations. The solution is generated from intensive iteration of these equations made possible only by the computer. CFD technique has become very useful for numerous projects. It can also be used to determine some parameters that are difficult to obtain by experiments.

CFD works by solving the equations of fluid flow over a region of interest, with specified conditions on the boundary of that region. The geometry or the dimensions are needed to construct the computational domain and generate the grid for the CFD models. The fluid properties are to be defined. Physical and chemical phenomena are selected. Appropriate boundary conditions and constraints need to be defined. With the specified operational parameters, simulations can be performed to identify flow behavior and turbulence quantities. External models such as bubble population balance model can be solved along with the governing equations for fluid flow and turbulence.

Advantages of CFD can be summarized as:
1. It provides the flexibility to change design parameters without the expense of hardware changes. It therefore costs less than laboratory or field experiments, allowing engineers to try more alternative designs than would be feasible otherwise.
2. It has a faster turnaround time than experiments.
3. It guides the engineer to the root of problems, and is well suited for trouble-shooting.
4. It provides comprehensive information about a flow field, especially in regions where measurements are either difficult or impossible to obtain.

2.3 Usage and Capabilities of CFD

In the recent years computational fluid dynamics (CFD) has been applied to bioreactors by various authors. Computational approaches can be used to identify critical constraints in geometry for scale-up or operation, simulate and optimize impeller rotational speeds, air sparging rates, mixing, gas hold-up and mass-transfer coefficients and distribution of gases within bioreactors. CFD is a simple way of predicting the power numbers of impellers which are difficult to be measured experimentally. In

addition CFD can optimize a bioreactor process by quantifying shear stresses, flow fields, and mass transfer characteristics.

Several recent publications have established the potential of computational fluid dynamics (CFD) for describing the hydrodynamics of stirred tank and improving the knowledge of local information about turbulent flow field, gas-holdup, interfacial area, and bubble size and reaction rates [7]. For example, Kumara Dhanasekharan [6] has shown the effective usage of CFD in determining hydrodynamic and mixing effects during scale-up of bioreactors and coupled with multiphase gas-liquid hydrodynamics and oxygen transfer in airlift and stirred tank bioreactors.

2.4 Mathematical Models in CFX

CFX is a commercial Computational Fluid Dynamics (CFD) program, used to simulate fluid flow in a variety of applications. It uses finite-volume approach to discretizing the Navier-Stokes equations. For the finite volume technique, the region of interest is divided into small sub-regions, called control volume. The equations are solved iteratively for each control volume. As a result, an approximation of the value of each variable at specific points throughout the domain can be obtained. ANSYS CFX supports arbitrary mesh topologies, including hexahedral, tetrahedral, wedge and pyramids elements. The governing equations vary according to the models selected. The geometry of fermenter studied in this project is a mixing tank. With the rotating impeller geometry, it is desired to use the moving reference frame modeling which is further discussed. Population balance equation is used to analyze the size distribution of the dispersed phase and accounting for the breakage and coalescence.

2.4.1 Eulerian multiphase model

Two phase flow phenomena occur in various industrial applications. The primary multiple-phase model of CFX code is the Eulerian Multiphase model. The governing equations in this approach can be derived by ensemble averaging the fundamental conservation equations for each phase to describe the motion of liquid and gas in the stirred tank [8]. It is derived from the single-phase model by introducing the volume fraction and a mechanism for the exchange of momentum between phases. The transport equations governing conservation of mass and momentum are derived for each phase and are solved simultaneously.

2.4.2 Mass conservative equation for two phase flow

A basic principle of science and engineering is the conservation of mass. The equation of continuity is developed by writing a mass balance over a stationary volume element through which fluid is flowing. The mass continuity equation describes the mass flux ratio into and out of a control volume and its internal change of mass. It can be expressed as:

$$\begin{bmatrix}\text{Rate of change}\\ \text{of mass in}\\ \text{control volume}\end{bmatrix} = \begin{bmatrix}\text{Rate of mass}\\ \text{convected into}\\ \text{control volume}\end{bmatrix} - \begin{bmatrix}\text{Rate of mass}\\ \text{convected out to}\\ \text{control volume}\end{bmatrix} \qquad (2.1)$$

This equation in vector notation is

$$\frac{\partial \rho}{\partial t} + \nabla(\rho v) = 0 \qquad (2.2)$$

Where, $\frac{\partial \rho}{\partial t}$: rate of increase of mass per unit volume

$\nabla(\rho v)$: net rate of mass addition per unit volume by convection

Two phase flow phenomena occur in various industrial applications. In this work, two-phase flow occurs in a system containing gas-liquid dispersion in stirred tank. The continuity equation for the flowing liquid and gas is written in terms of the accumulation and convection terms balanced by the total mass transferred to and from the other phases. The continuity equation for a phase, 'α', in a multiphase flow problem is as follows:

$$\frac{\partial}{\partial t}(r_\alpha \rho_\alpha) + \nabla.(r_\alpha \rho_\alpha v_\alpha) = S_\alpha + \sum_{\beta=1}^{Np} \Gamma_{\alpha\beta} \quad (2.3)$$

Where, r_α : Phase volume fraction
ρ_α : Phase density
v_α : Phase velocity
S_α : Mass sources
$\Gamma_{\alpha\beta}$: Mass flow rate per unit volume from phase β to α
N_p : Number of phase

The left-hand side describes the internal change of mass over time and the convective flux crossing the boundaries of the control volume. The first term of right-hand side (S_α) describes the user specific mass source. $\Gamma_{\alpha\beta}$ term only occurs if interphase mass transfer take place. Where r_α is the volume fraction of phase α, which needs to satisfy the Eq. (2.4)

$$\sum_{A=1}^{Np} r_\alpha = 1 \quad (2.4)$$

One of the most important characteristics of a multi-phase system is fractions of various phases. Thus, it is necessary to know the volume fraction in the entire computational domain. In this work, the liquid phase (L) and gas phase (G) are assumed to share space in proportional to their volume. Therefore, volume fraction equation is:

$$r_l + r_g = 1 \quad (2.5)$$

2.4.3 Momentum conservation equation

The momentum equation is a statement of Newton's Second Law. Newton's second law of motion may be stated as follows: The time rate of change of momentum of a system is equal to the net force acting on the system, and takes place in the direction of the force. It can be expressed as:

$$\begin{bmatrix}\text{Sum of forces}\\ \text{acting on}\\ \text{control volume}\end{bmatrix} = \begin{bmatrix}\text{Rate of momen}-\\ \text{tum out of}\\ \text{control volume}\end{bmatrix} - \begin{bmatrix}\text{Rate of momen}-\\ \text{tum into}\\ \text{control volume}\end{bmatrix} + \begin{bmatrix}\text{Rate of accumulation}\\ \text{of momentum with}\\ \text{in control volume}\end{bmatrix} \quad (2.6)$$

The momentum equation for multiphase flows is described by the Navier-Stokes equation. It is derived from the single-phase model by introducing the volume fraction and a mechanism for the exchange of momentum between phases. The fundamental conservation equations are modified and applied to each phase. For the fluid-fluid multiphase flow, the conservation of momentum for a phase α is

$$\frac{\partial}{\partial t}(r_\alpha \rho_\alpha v_\alpha) + \nabla.(r_\alpha(\rho_\alpha v_\alpha \otimes v_\alpha)) = -r_\alpha \nabla p_\alpha + \nabla.(r_\alpha \mu_\alpha(\nabla v_\alpha + (\nabla v_\alpha)^T) + \sum_{\beta=1}^{Np}(\Gamma^+_{\alpha\beta} v_\beta - \Gamma^+_{\beta\alpha} v_\alpha) + S_{M\alpha} + M_\alpha \quad (2.7)$$

Where, $S_{M\alpha}$: momentum sources due to external body forces

M_α : Interfacial forces acting on phase α due to the presence of other phases

$(\Gamma^+_{\alpha\beta} v_\beta - \Gamma^+_{\beta\alpha} v_\alpha)$: momentum transfer induced by interphase mass transfer

2.4.4 Turbulence modeling

Turbulence consists of fluctuation in the flow field in the time and space. It is a complex process, mainly because it is in three dimensional, unsteady and consist of many scales. It can have a significant effect on the characteristics of the flow. Turbulence occurs when the inertia forces in the fluid become significant compared to viscous forces, and is characterized by a high Reynolds number.

The turbulence modeling can be done using various options. Two-equation turbulence model are very widely used, as they offer a good compromise between numerical effort and computational accuracy. The turbulence equations include an effective viscosity in order to include the effects of turbulent eddies. The flow is affected due to turbulence because of the effective viscosity. The standard k – ε model is used in this case for the turbulence modeling which is popularly used for recirculating flows. In two-equation models, the turbulence velocity scale is computed from the turbulent kinetic energy, which is provided from the solution of its transport equation. The turbulent length scale is estimated from two properties of the turbulence field, usually the turbulent kinetic energy and its dissipation rate. The dissipation rate of the turbulent kinetic energy is provided from the solution of its transport equation [15].

2.4.4.1 The k-epsilon model

The k-epsilon model is one of the most common turbulence models. It includes two extra transport equations to represent the turbulent properties of the flow. The first transported variable (k) is the turbulence energy and is defined as the variance of the fluctuations in velocity. It has dimensions of L^2T^{-2}. The second transport variable (ε) is the turbulence eddy dissipation (the rate at which the velocity fluctuations dissipate), and has dimensions of L^2T^{-3}. Single phase k- ε turbulence model is extended to multiphase turbulence model for continuous liquid phase by solving the following transport equation;

$$\frac{\partial}{\partial t}(r_l \rho_l k) + \nabla.\left(r_l\left(\rho_l \mu_l k - \left(\mu + \frac{\mu_{tl}}{\sigma_k}\right)\nabla k\right)\right) = r_l(P_l - \rho_l \varepsilon) \quad (2.8)$$

$$\frac{\partial}{\partial t}(r_l \rho_l \varepsilon) + \nabla.\left(r_l \rho_l \mu_l \varepsilon - r_l\left(\mu + \frac{\mu_{tl}}{\sigma_\varepsilon}\right)\nabla \varepsilon\right) = r_l \frac{\varepsilon}{k}(C_{\varepsilon 1} P_l - C_{\varepsilon 2} \rho_l \varepsilon) \quad (2.9)$$

The k- ε model assumes that the turbulence viscosity is linked to the turbulence kinetic energy and dissipation via the relation:

$$\mu_{tl} = c_\mu \rho_l \frac{k^2}{\varepsilon} \quad (2.10)$$

Where, μ : molecular (dynamics) viscosity (kg m^{-1} s^{-1})

μ_{tl} : liquid phase turbulence viscosity (kg m^{-1} s^{-1})

c_μ : turbulence model constant depending on the model used
k : turbulent kinetic energy (m^2s^{-2})
ε : the turbulent dissipation rate (m^2s^{-3})

2.5 Population Balance Equation

For gas-liquid stirred tanks, most of reports have made assumption that gas bubbles have the same size and shape. However, a wide spectrum of bubble sizes and shapes exist at different points throughout the whole reactor. As gas bubbles with different sizes and shapes experience different forces, which result in different velocities and volume fraction distributions for gas phase. The differences of volume fraction distribution and velocities have an effect on the gas bubble sizes and shapes too [10].

A realistic local bubble size distribution is the key factor in successful modeling of gas interactions and mass transfer rate. Population balance is a well-established method used to analyze the size distribution of the dispersed phase and accounting for the breakage and coalescence effect.

A standard two-phase flow calculation, with equations for continuity, momentum and turbulence for a continuous and a dispersed phase, can be extended to include equations for the mass fraction of bubbles within several size ranges using the Multiple Size Group model (MUSIG). These size fractions provide a more accurate measure of the interfacial area density and, therefore, allow better calculation of the heat and mass transfer taking place between the continuous and dispersed phases [15].The MUSIG model available in commercial code CFX is based on population balance method and two-fluid modeling approach. The main assumption of the MUSIG model is that all bubble size groups share a common velocity field but with different slip velocities for different size bubbles: this allows the computational cost to be reduced. The general form of the population balance equation is:

$$\frac{\partial n_i}{\partial t} + \nabla.(v n_i) = B_b - D_b + B_c - D_c \qquad (2.11)$$

Where, n_i : the number of group-i particles per unit volume
B_b and B_C : the birth rate due to break-up and coalescence respectively
D_b and D_c : death rates due to break-up and coalescence respectively

The dispersed phase is divided into N size class. For each class, a continuity equation taking into account of the inter-class mass transfer resulting from particle and break-up is derived from the population balance equation. Normally, typical simulation is desirable to set the number of bubble-classes as low as possible, because solving population balances are computationally time consuming. However, if the number of classes is too low, the simulation is likely crash due to high coalescence and breakage rates [16]. The size groups of each class bubble are divided based on the criteria of equal diameter. The bubble diameter of group i is calculated from equation (2.12).

$$d_i = d_{min} + \Delta d\left(i - \frac{1}{2}\right) \; ; \; \Delta d = \frac{(d_{max} - d_{min})}{N} \qquad (2.12)$$

Where, d_{max} : maximum diameter of dispersed phase
d_{min} : minimum diameter of dispersed phase

2.6 Multiple Reference Frames Technique and Sliding Mesh Technique

For simulation of impeller motion, there are two common techniques which are multiple reference frame model (MRF) technique and sliding mesh technique (SM). The SM approach is a fully transient approach, where the rotation of the impeller is explicitly taken into account. On the other hand, the MRF approach predicts flow for fixed position of the impeller blades relative to the tank baffles. The rotational motion of the impeller is then replaced by the centrifugal forces when the momentum equation is solved in the impeller region [12]. The SM approach is more accurate but it is also much more time-consuming than the MRF approach. In this work, in order to save calculation time, the MRF approach is selected.

In the MRF technique, the computational domain is divided into two zones. For the inner zone with the impeller, a rotational reference frame is defined, and for the outer zone, which includes the baffles, a fixed inertial reference frame is defined. Fluid motion in a rotating subdomain is solved in a rotating frame, and the solution is matched at the interface between the rotating and stationary regions via velocity transformations from one frame to the other. The “velocity matching” step implicitly involves the assumption of steady flow conditions at the interface, but permits multiple fluid (not grid) regions to rotate relative to each other.

The assumption of a steady flow condition at the interface of MRF approach is suited to situations where relatively weak interactions can be found, such as baffled mixing tank with enough spacing between the impellers and baffles.

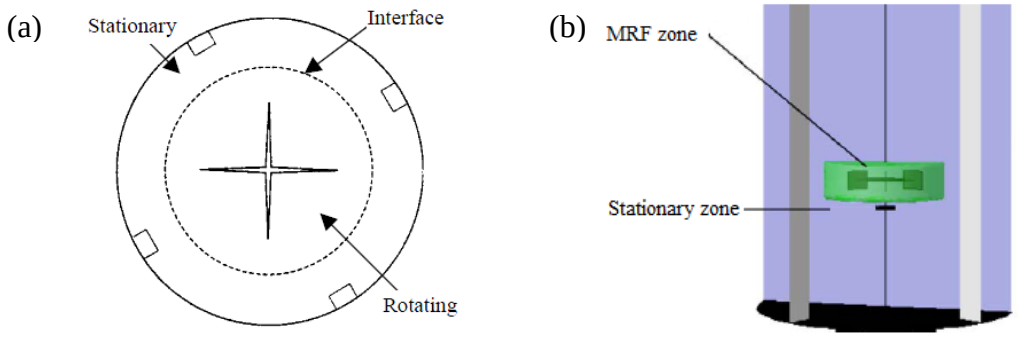

Figure 2.2 (a) MRF representation of rotor/stator interaction (b) The computational domain used in the CFD model

The influence of rotating domain size of rotating impeller in a mixing vessel on the accuracy of results was studied by Zadravec et al [17]. In this study, the CFD simulations of the mixing vessel equipped with Rushton turbine were done using MRF technique with four difference size of rotating domain. The simulation results were compared with experimental results from Particle Image Velocimetry (PIV) system. From the results, it can be conclude that the simulation model with the largest rotating domain size is the most accurate in following the experimental results. The numerical error due to interpolation of the results between both domains is decreased by enlarging the size of the rotating domain. The position of interface should avoid intersecting the highest flow velocities region made by impeller.

2.7 Theory

2.7.1 Oxygen requirement of fermentation

The high oxygen demand of the methanol metabolism makes oxygen supply a major control parameter in *P. pastoris* culture. In the methanol-containing media, *P. pastoris* uses methanol by the oxidative pathway only in the presence of sufficient amounts of oxygen and consumes methanol as a carbon source [18]. Considering the methanol metabolism in *P. pastoris*, the oxygen limitation is generally supposed to negatively affect cell growth. Additionally reported for fermentation of Pachysolen tannophilus, the actual growth of the organism on D-xylose as well as on D-glucose is still dependent on the availability of oxygen. The relative percent of oxygen in the medium is referred by dissolved oxygen. In fermentation of *P. pastoris*, DO must be kept above a minimal level, generally about 20%. Excessively high DO levels are cytotoxic and significantly reduce cell viability. Because of the high cost of oxygen, maintaining high levels of DO can in some cases be economically unfeasible. The amount of DO into broth is limited by its solubility, mass transfer rate and consumption of microorganisms.

2.7.2 Mass balance for the dissolve oxygen

The mass balance for dissolve oxygen in the well mixed liquid phase can be established as:

$$\frac{dC}{dt} = OTR - OUR \tag{2.13}$$

Where, dC/dt : the oxygen accumulation rate in the liquid phase.
OTR : the oxygen transfer rate from gas to liquid.
OUR : the oxygen up take rate by microorganisms.

Oxygen up take rate can be express by:

$$OUR = q_{o_2}.C_x \tag{2.14}$$

Where, q_{o_2} : the specific oxygen uptake rate of the microorganism employed (moles O_2/g cells.s)
C_x : biomass concentration (g cell mass/m^3)

2.7.3 Oxygen transfer in fermenter

For aerobic fermentation, oxygen transfer is a key variable. Oxygen transfer is a function of aeration and agitation. Aeration is the supply of oxygen-containing air into the fermenter. Agitation is the stirring of the broth to achieve improved distribution of the air bubble rising from the bottom of the fermenter. The solubility of oxygen in aqueous solution is low. In pilot-scale and product-scale fermentation, oxygen transfer becomes the limiting factor for the growth of the microorganism. The main factors affecting the mass transfer rate in gas-liquid dispersions are the sparger design, the diameter of the orifice, the tank design, the type of agitator and its relative dimensions, the power input, the gas flow rate, and physical and chemical properties of the liquid (interfacial area of gas bubbles, medium composition and oxygen partial pressure) [19]. Several researchers have studied the hydrodynamics of bubbles and mass transfer in bioreactors.

During aerobic bioprocess, the oxygen is transferred from a rising gas bubble into a liquid phase and uptake by cell. The transport of oxygen from air bubbles to the cells can be represented by a number of steps:

(i) The transfer of oxygen from an air bubble into solution.
(ii) The transfer of the dissolved oxygen through the fermentation medium to the microbial cell.
(iii) The uptake of the dissolved oxygen by the cell.

The oxygen mass transfer from gas to liquid can be described and analyze by means of volumetric mass transfer coefficient, k_La. It represents the most important parameter implied on the design and operation of mixing of the bioreactors. Rate of mass transfer is directly proportional to the driving force for transfer and the area available for the transport process to take place. Therefore, rate of oxygen transfer from air bubble to the liquid phase may be described by the equation:

$$\text{Oxygen Transfer Rate (OTR)} = k_La\ (C^* - C_L) \quad (2.15)$$

Where,
- C_L : concentration of dissolved oxygen in fermentation broth (mmoles dm^{-3})
- t : time (h)
- k_L : liquid-phase mass transfer coefficient (cm h^{-1}).
- a : gas-liquid interface area per liquid volume (cm^2 cm^{-3})
- C* : saturated dissolved oxygen concentration (mmols dm^{-3})

It is clear that three parameters are involved in the oxygen transfer rate. It is extremely difficult to measure both 'k_L' and 'a' during fermentation and, therefore, the two terms are generally combined in the term k_La, the volumetric mass-transfer coefficient, having units of reciprocal time (h^{-1}). The driving force is the gradient between the saturated dissolved oxygen concentration and concentration of dissolved oxygen in fermentation. Factors affecting this gradient include the solubility and metabolic activity. The gas solubility, C*, in electrolyte solutions is usually smaller than the gas solubility in pure water ("salting-out effect"). Gas solubility is mainly dependent on the temperature, the pressure, concentration and type of salts present and the chemical reactions [20].

2.7.4 Volumetric mass transfer coefficient

The volume mass-transfer coefficient is used as a measurement of aeration capacity of fermenter. The larger of the k_La value means the higher the aeration capacity of the system. The most important characteristics affecting the mass transfer between the gas-liquid phases are the energy dissipated by turbulence, the gas hold-up, the size of the bubbles or their distribution within the volume being mixed. Those variables are a function of operational conditions (power input or stirrer speed and gas flow), physical properties of the solution and gas phase (viscosity, surface tension and density) and the geometry of the vessel, mainly the stirrer and the gas distributor [21].

In a bioreactor, the transport of oxygen from gas phase to liquid phase is controlled by the liquid-phase mass-transfer coefficient, k_L. To determine the total oxygen transfer rate in a fermenter, the total surface area available for mass transfer, a, has to be known. Separate determination of k_L and a is difficult to evaluate and sometimes impossible. The combined term of k_La is usually reported as the mass-transfer coefficient rather than just k_L [22].

In this research, Higbie's penetration theory and eddy cell model were used for calculating k_L as a function of spatial position in a tank. The liquid-phase mass transfer coefficients for a bubble from these two theories are given by:

Higbie's penetration
$$k_L = \frac{2}{\sqrt{\pi}} \sqrt{D} \left(\frac{\varepsilon.\rho_L}{\mu_L}\right)^{1/4} \quad (2.16)$$

Eddy cell model
$$k_L = 0.3 \sqrt{\frac{D.\rho_L}{\mu_L}} \left(\frac{\varepsilon.\mu_L}{\rho_L}\right)^{1/4} \quad (2.17)$$

Where, ε : the water turbulent energy dissipation rate that can be predicted from a CFD simulation
D : the diffusion coefficient

The interfacial area is also directly obtained from the predicted bubble size distribution as:

$$a = \frac{6\alpha_g}{d_{32}} \quad (2.18)$$

Where, α_g : gas hold up.
d_{32} : sauter mean diameter

The bubble size distribution was defined by the sauter mean diameter:

$$d_{32} = \frac{\sum_i n_i d_i^3}{\sum_i n_i d_i^2} \quad (2.19)$$

Where, n_i : the number of bubbles having an equivalent diameter d_i.

2.7.5 Solubility of oxygen

The solubility of oxygen in the broth is a function of the media composition, temperature and pressure. The total pressure and the oxygen partial pressure used during the aeration of the broth affect the value of the solubility of the dissolved oxygen. For solutions, the equilibrium relationship between these parameters follows Henry's Law.

$$p_{o_2} = p.y_{o_2} = HC^*_{o_2} \quad (2.20)$$

Where, p : gas phase pressure (Pa)
p_{o_2} : partial pressure of O_2 in the gas phase (Pa)
y_{o_2} : mole fraction of O_2 in the gas phase
H : Henry's law constant
$C^*_{O_2}$: saturated dissolved O_2 concentration (mol/l)

If the total pressure or the concentration of oxygen is increased at constant temperature, the solubility increases and therefore the mass transfer also increase.

2.7.6 Scale up strategies in aerobic bioprocess

Once a bioprocess is accomplished successfully in laboratory scale experiments, the values of the operating variables and the physical properties are known or can be

measured. The bioprocess is then usually carried out on increasing scale reactors. There are several scale-up methods, which can be applied to fermentation process carried out in aerated bioreactors. The different scale-up criteria normally result in different process conditions on a production scale. The rules of thumb method is the most common method. The scale-up criterions most frequently used are constant specific power input (P_g/V_L), constant k_La, constant tip speed of the agitator and constant air velocity [23]. However, it is not possible to keep all cultivation parameters constant upon converting the process to a larger scale. Therefore, the most important parameter of the fermentation process has to be chosen as the scale-up criterion. In most cases, the nature of the process and the properties of the microorganism dictate this choice.

2.7.6.1 Scale-up on basis of constant oxygen transfer coefficient, k_la

The most commonly used scale-up for fermentations limited by oxygen transfer is on the basis of constant k_La or constant oxygen transfer rate. Scale-up of aerobic fermentations is often carried out in this basis to ensure the same oxygen supply rate to support normal growth of cell. Often, the supply of oxygen is the factor limiting the productivity of the fermentation process, especially in high density cultivation. If the oxygen transfer is a limiting cultivation parameter, scale-up is most often performed by keeping the oxygen transfer constant. On this basis, the k_La value is kept constant upon scale-up to maintain similar mass-transfer of oxygen at the larger production scale. This will achieve the same growth rate in the scaled-up fermenter.

2.7.6.2 Scale-up on basis of constant power consumption per unit liquid volume

Scale-up on the basis of constant power input per unit liquid volume is widely practiced. This method is a strong candidate for use as a criterion for bioreactor design and process scale up. Volumetric power consumption is defined as the amount of energy required to generate movement of a fluid within a vessel in a given period of time. This criterion is commonly used for scale up in the bioprocess, especially in the process that contains shear sensitive operation and in an aerobic fermentation where gas dispersion in bioreactor is an importance factor [23]. According to Rushton equation the power input for the agitation of a non-aerated mixture, P_o is characterized by the dimensionless variable power number (N_P) [3]:

$$P_o = N_P \rho N^3 D_i^5 \quad (2.21)$$

Where, N : impeller speed (s^{-1})
D_i : impeller diameter (m)
N_P : power number
P_o : ungassed power consumption (w)

For equal power per unit volume, the following equation expresses relations between the impeller size and agitation rate in small and large bioreactors.

$$\frac{P_{o1}}{V_1} = \frac{P_{o2}}{V_2} \quad (2.22)$$

For geometrically similar vessels in the region of turbulent flow where P_o/V is constant, Equation 2.22 becomes

$$\frac{\rho N^3 D_i^5}{D_i^3} = \frac{\rho N^3 D_i^5}{D_i^3} \tag{2.23}$$

$$N_1^3 D_{i1}^2 = N_2^3 D_{i2}^2 \tag{2.24}$$

The agitation rate is proportional to impeller diameter to power of 2/3.

$$N_2 = N_1 \left(\frac{D_{i1}}{D_{i2}}\right)^{2/3} \tag{2.25}$$

The power consumption in ungassed systems is always higher than the power consumption in gassed systems, since aeration significantly influences the power drawn from the impeller by the fluid. Michel and Miller (1962) suggest the following relationship for estimating the volumetric power consumption:

$$P_g = m \left(\frac{P_0^2 N D_i^3}{Q^{0.56}}\right)^{0.45} \tag{2.26}$$

Where, P_g : gassed power consumption
Q : Volumetric air flow rate

Substitution of Equation 2.21 in Equation 2.26 gives the equation:

$$P_g = m \left(\frac{N_p^2 \rho_L^2 N^7 D_i^{13}}{Q^{0.56}}\right)^{0.45} \tag{2.27}$$

For equal power per unit liquid volume

$$\frac{P_{g1}}{V_1} = \frac{P_{g2}}{V_2} \tag{2.28}$$

If geometrically similar vessels are employed in scale-up, the value of the geometry dependent constant will be the same for both scales, thus:

$$\frac{P_{g1}}{\frac{\pi D_{T1}^2 H_{T1}}{4}} = \frac{P_{g2}}{\frac{\pi D_{T2}^2 H_{T2}}{4}} \tag{2.29}$$

$$\frac{P_{g1}}{D_{i1}^3} = \frac{P_{g2}}{D_{i2}^3} \tag{2.30}$$

Substituting P_{g1} and P_{g2} for both scales into Equation 2.30, the following equation is used for scaling-up on basis of constant gassed power input per unit liquid volume:

$$\frac{N_1^{3.15} D_{i1}^{5.85}}{Q^{0.252} D_{i1}^3} = \frac{N_2^{3.15} D_{i2}^{5.85}}{Q^{0.252} D_{i2}^3} \tag{2.31}$$

$$\frac{N_1^{3.15} D_{i1}^{2.85}}{Q_1^{0.252}} = \frac{N_2^{3.15} D_{i2}^{2.85}}{Q_2^{0.252}} \quad (2.32)$$

2.7.6.3 Scale-up on basis of constant superficial air velocity, v_g

Superficial air velocity is defined as gas flowrate divided fermenter cross-sectional area. In scaling up on the basis of constant power consumption per unit liquid volume, it is therefore necessary to alter the volumetric air flowrate in order to maintain a constant superficial air velocity on both scales of operation. The required air flow rate on the larger scale may be calculated by using Equation 2.33.

$$v_{g1} = v_{g2} \quad (2.33)$$

Superficial air velocity,

$$v_g = \frac{4Q}{\pi D_t^2} \quad (2.34)$$

Therefore, equation 2.33 becomes:

$$\frac{4Q_1}{\pi D_{t1}^2} = \frac{4Q_2}{\pi D_{t2}^2} \quad (2.35)$$

Thus, with geometrically similar vessels, the required volumetric air flowrate is:

$$Q_2 = Q_1 \left(\frac{D_{T2}}{D_{T1}}\right)^2 \quad (2.36)$$

2.7.6.4 Scale-up on basis of constant Impeller tip speed

For shear-sensitive fermentation broths, constant tip speed is the best approach. Tip speed influences impeller shear, which is proportional to the product of impeller tip speed and impeller diameter for turbulent flow conditions. If scale-up is carried out using constant tip speed (with geometric similarity), the value of P/V is often lowered, which can adversely affect aeration efficiency. In this method, the impeller tip speed is maintained at a constant value during scale-up. Thus,

$$V'_{i1} = V'_{i2} \quad (2.37)$$

Where, Impeller tip speed, $V'_i = \pi N D_i$

Equation 2.37 becomes,

$$\pi N_1 D_{i1} = \pi N_2 D_{i2} \quad (2.38)$$

Therefore, the required impeller speed for larger scale is as follows:

$$N_2 = N_1 \left(\frac{D_{i1}}{D_{i2}}\right) \quad (2.39)$$

In practical application, all four methods are used in combination with each other and sometimes the trial and error method must be also included. It is impossible to keep all operation condition in the same ratio [24]. It is necessary to choose which variable is considered as the most important. For the scale-up of aerobic fermentation, the effe
gas liquid mass transport is the most significant factor. Therefore, scale-up in aerobic fermentation is often performed on the basis of keeping the volumetric mass transfer coefficient.

CHAPTER 3 METHODOLOGY

This research used CFD simulation technique to investigate the hydrodynamics and mas transfer in a bioreactor. The commercial code ANSYS CFX version 13 was used to simulate gas-liquid flow in aerated stirred bioreactor. The population balance model (PBM) described in chapter 2 was used for accounting the formation, coalescence, break-up and death of the bubbles. The CFX simulation processes consist of three steps which are pre-processing, solving and post-processing. The models of bioreactors were developed in the geometry creation tool, ANSYS Design modeler. After that, two phase simulation of 2L bioreactor was performed. The CFD model prediction of the mass transfer coefficient of 2L bioreactor was compared with the experimental result. The gassing out technique was performed to determine the mass transfer coefficient with the same operation condition used in CFD simulation. Using this technique, the mass transfer coefficient values of 2L bioreactor were calculated at different impeller speed. Last step, the scale up study based on the constant oxygen mass transfer coefficient from 2L to 200L bioreactor was performed. Ultimately, the CFD model of 200L bioreactor was created with the same technique of 2L bioreactor. The details of 2L and 200L bioreactors and the impellers are given in this chapter.

3.1 Steps of simulation process

The steps of simulation process are shown in Figure 3.1. The first step of simulation processes is to create geometry and mesh of the bioreactor model. Creating the geometry is the first part of the first step where the geometry is described and the dimensions are set. The second part of the first step is meshing, where the geometry created in the first part is to be discretized to small elements of Hexahedral, Tetrahedral or Pyramid. Then, the mesh file generated in Design modeler is imported into ANSYS CFX to start the pre-processing step. Pre-processing covers all the tasks that take place before the numerical solution process. This step involves defining the flow domain, setting the fluid properties, applying the boundary conditions, specifying initial conditions and setting the numerical control parameters. All this information is fed to the solver programs of the software, which then solves the numerical equations and produces the results. The last step of the simulation is the post processing where obtained results are displayed and analyzed in the post-processor in various ways such as vector plots, graphs, and contours.

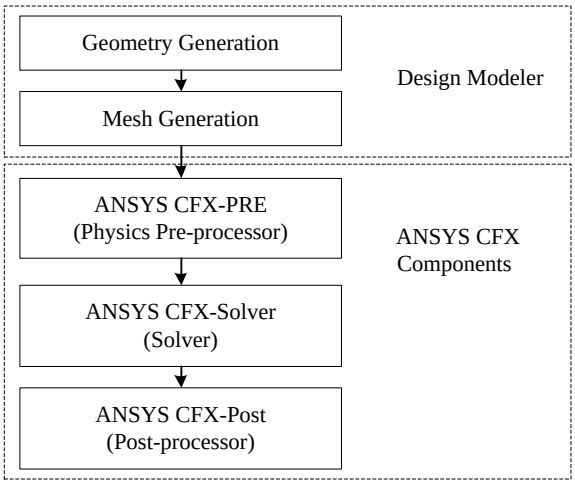

Figure 3.1 The steps of the simulation of CFD process

3.1.1 Creating Geometry

A commercial grid-generation tool, Design modeler, was used to model the geometry of bioreactors. For the present study, multiple frame of reference (MFR) approach was used. It is one of the widely used methods in the literature for simulating the flow field in stirred reactors. In this approach, the geometry of tank is divided into two regions. The first region is a rotating frame which encompasses the impeller and the flow surrounding it. The second region is a stationary frame which includes the tank, baffles and the flow outside the impeller frame.

3.1.2 Meshing Geometry

The entire basis of CFD is formed on discretizing a fluid volume into cells and using a finite volume technique to approximate fluid properties in each of those cells. The spatial discretization is referred to as meshing or creating a mesh. There are several software packages used for meshing geometry, but for this study the ANSYS ICEM CFD was used. The basic building blocks for 3D mesh are tetrahedron, hexahedron, pyramid and prism. In order to account for the efficient modeling using Multiple Reference Frames (MRF), a very fine mesh is required for the rotating impellers. The accuracy of the solution depends on the quality of meshing. However, the increasing of the number of cells will affect the computational time and complexity of the simulations. Therefore, the suitable mesh type must be selected.

3.1.3 Pre processing

After the meshing model step was performed, the mesh file is transferred to ANSYS CFX program to simulate and solve problem. Pre-processing is the process which is used to create input required by the solver. In this step, the physical models that are to be included in the simulation are selected. Fluid properties of liquid phase and boundary conditions and initial conditions must be defined.

3.1.4 Solving

This is the step where CFX starts to solve the simulation of the process. At the end of iteration, an approximate solution is calculated for the problem. The solving step will terminate when the solution converge, i.e., relative error is less than the specified value or when the number of iterations reaches the user specified value.

3.1.5 Post-processing

The post processor is the component used to analyze and display the results. There are many different types of outputs depending on the needs of the simulation. Contour, charts and graph are the most common. Visualization tools can be used to study the overall flow pattern, separation, shear layers and also about the consistency of the result from a common knowledge of the system.

3.2 Simulation of 2L bioreactor

3.2.1 Creating geometry of 2L bioreactor

The detail of the 2L bioreactor geometry is taken from BIOSTAT B (Braun Biotech) ellipsoidal-bottom cylindrical vessel. All internal dimensions are presented in Table 3.1. The vessel is 13 cm in diameter and 16.3 cm in height and equipped with four baffles. There are two Ruston turbines along the shaft which are located at the center of the reactor. Each turbine was made by six blades and having 1 mm of thickness. The bottom impeller was set at the distance of 4.5 cm above the tank bottom. The clearance between two impellers is 50 cm. Compressed air was introduced below the bottom impeller through gas sparger. A 4 cm diameter ring type gas sparger was employed, with 14 holes of 0.5 mm in diameter located 1 cm above the bottom of vessel.

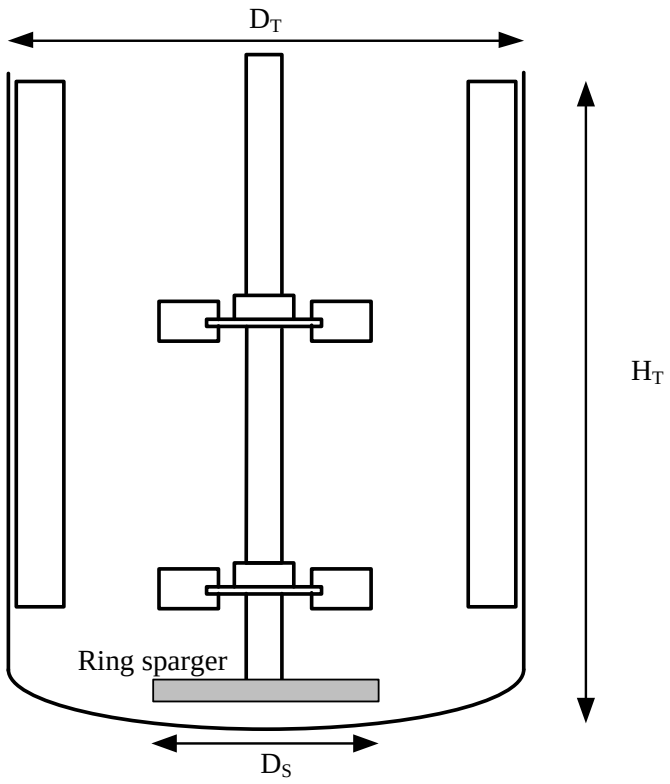

Figure 3.2 Geometry of 2 L bioreactor

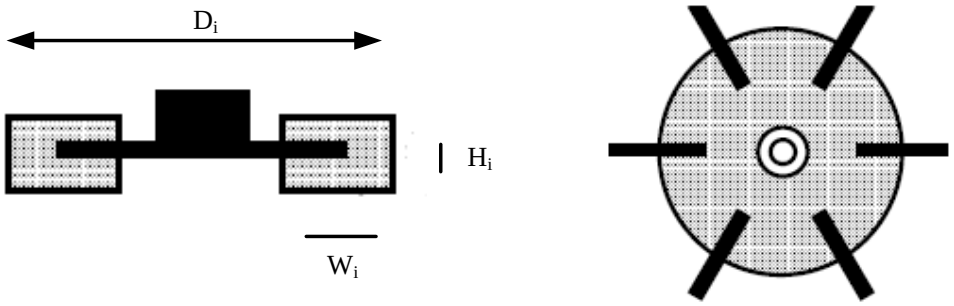

Figure 3.3 Geometry of Rushton impeller of 2 L bioreactor

Table 3.1 Important dimensions of 2L bioreactor

Dimension	2 Liter Bioreactor
Total volume, V_T (L)	3
Working volume, V_L (L)	0.6-2
Vessel height, H_T (mm)	170
Vessel diameter, D_T (mm)	130
Impeller type	Rushton Turbine
Number of impellers	2
Impeller diameter, D_i (mm)	53
Impeller thickness, T_i (mm)	1
Impeller width, W_i (mm)	15
Impeller height, H_i (mm)	10
Spacing between lower impeller and tank bottom (mm)	50
Spacing between impeller, Δ_C (mm)	70
Type of sparger	Ring sparger
Sparger diameter, D_S (mm)	40
Sparger distance from bottom (mm)	10
Number of hole	14
Hole diameter (mm)	0.5

Baffle height (mm)	140
Baffle width (mm)	10
Baffle thickness (mm)	1
Spacing between baffle and tank bottom (mm)	30

In order to saving CPU time, only half of vessel along the vertical axis was considered as solution domain. The three blades of impeller were located at an angle of 30^o, 90^o and 150^o. Two baffles were located at an angle 45^o and 135^o. As mentioned in section 2.7, for present study, we used the multiple frames of reference for simulating the flow field in stirred reactor. Therefore, three parts must be created which consist of Tank, Impeller 1 and Impeller 2. Through ANSYS CFX 13, Design Modeler is used as geometry generator. The tank part is the first part to be modeled. This part consists of tank, baffles gas sparger ring and some part of shaft. Both impeller parts consist of three blades and some part of shaft. The geometry of tank part and impeller part were shown in Figure 3.4, 3.5 and 3.6.

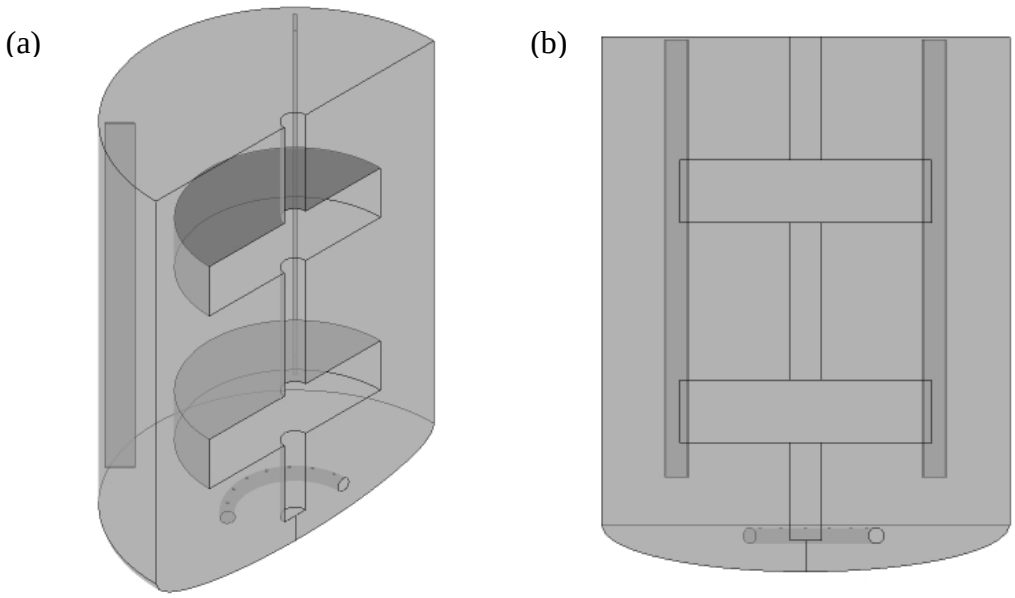

Figure 3.4 The geometry of tank part of 2 L bioreactor showed in (a) isometric view (b) front view

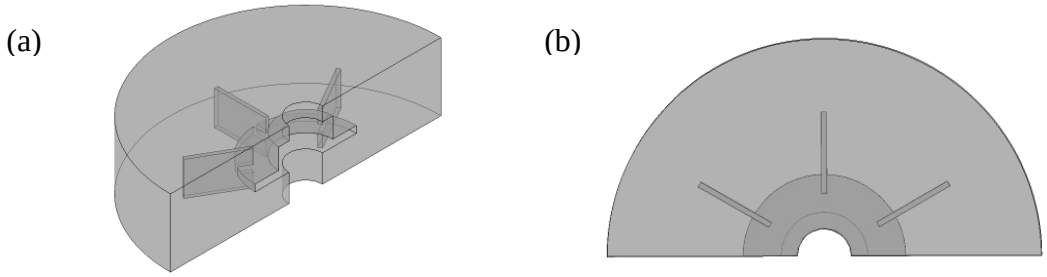

Figure 3.5 The geometry of impeller part of 2 L bioreactor showed in (a) isometric view (b) top view

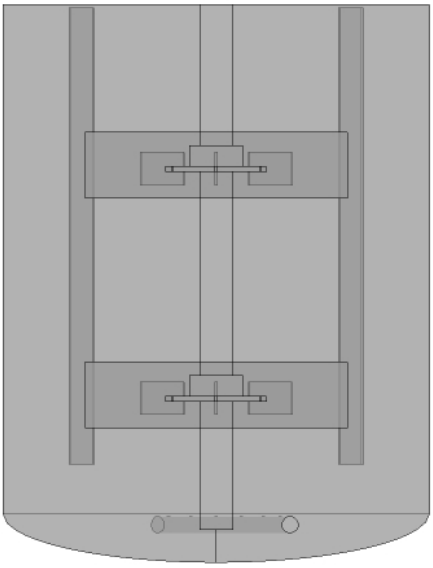

Figure 3.6 Solution domain of 2 L bioreactor showed in front view

3.2.2 Meshing geometry of 2L bioreactor

A commercial grid generation tool, ICEM CFD, was used to generate the computational grid. The Tank domain and impeller domains are discretized by hexahedral finite volume method. It is very important to use an adequate number of computational grids to ensure an adequate prediction of turbulence quantities. The quality of mesh, type mesh and number of computational grid of each part were shown in the Table 3.2. The computational grid used for this simulation is shown in Fig. 3.7 and 3.8.

Table 3.2 Meshing details of each part of 2 L bioreactor

	Type of mesh	Number of element	Average quality
Tank	Hexahedral	80124	0.72
Impeller 1	Hexahedral	14528	0.62
Impeller 2	Hexahedral	14528	0.62

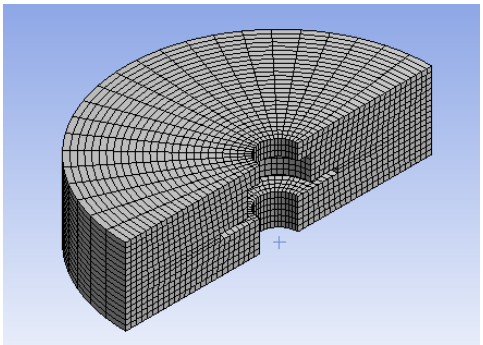

Figure 3.7 Computational gird of impeller part of 2 L bioreactor showed in isometric view

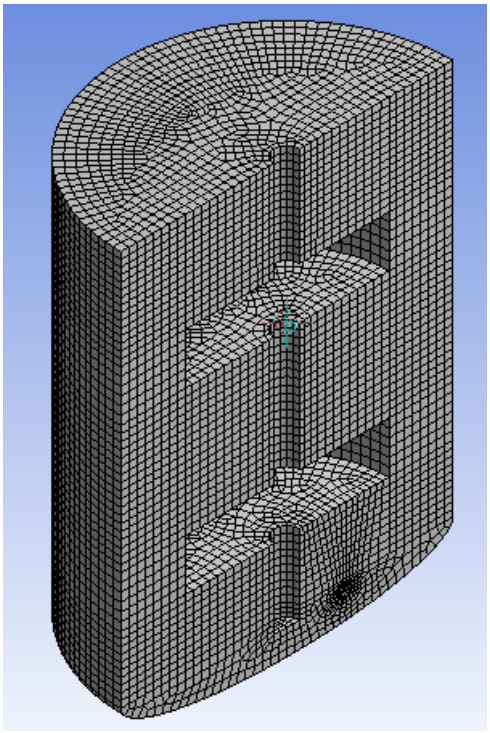

Figure 3.8 Computational gird of tank part of 2 L bioreactor showed in isometric view

3.2.3 Definition of boundary conditions of 2L bioreactor

The first step is defining a domain for the bioreactor. Steady state simulation is performed in this work. The domain motion is stationary for tank domain and rotating for both impeller domains. The flow in reactor is assumed as an isothermal process. Therefore no heat transfer occurs in the system and no energy equation is solved. Liquid phase is selected as continues fluid. Air is the dispersed fluid. The top surface of tank is considered as the degassing boundary condition for gas removal. The air flow rate at the sparger is specified as inlet boundary condition with gas volume fraction equal to 1. No slip boundary condition is applied on the baffles, tank wall, shaft and impellers. For the drag force, Grace Drag force Model is chosen because it is the optimum choice for Air Water system. In this simulation, the turbulence was modeled by using the k-ε turbulence model, which was a commonly used model. The main advantages of the k-ε turbulence model are short computation time, stable calculations, reasonable results for many flows and suitable for a wide range of applications. Heat transfer of the fluid model was not concerned in this research so the heat transfer of this model was neglected by selecting no heat transfer option in the default domain setting in order to save the simulation time. Multiple size group model function is used to predict the size of bubble which has large variation in its size. Bubbles ranging from 0.5 mm to 10 mm diameter are equally divided into 10 size group. High – resolution advection scheme was selected for solver control. This method gives high accuracy than upwind advection method. From the CFX manual, they do not recommend using upwind advection scheme to obtain final results. Upwind advection scheme was suitable for obtaining an initial set of results for the other complex simulation case. The convergence criterion is $1x10^{-4}$ of the residual target used in all simulation in order to obtain accurate result. The details of specifications of 2L bioreactor model were shown in Appendix C.

3.3 Experiments for Overall Mass transfer coefficient determination.

An experiment was performed at a working volume 2L in a bioreactor (Biostat B, Braun Biotech). The operating temperature was set to 25 ^{o}C. Three different agitation speeds was performed in this experimental which are 700, 800 and 900 rpm. The total gas flow rate for all experiments is 1.5 vvm (volume gas per volume medium and minute). *P.pastoris* chemostat medium used in this experiment contained per liter: 50 g glucose.H_2O, 0.9 g critic acid, 4.35 g $(NH_4)_2PO_4$, 0.01 g $CaCl_2.2H_2O$, 1.7 g KCl and 0.65g $MgSO_4.7H_2O$. The density of medium was determined by using pycnometer and the viscosity was determined using HAAKE viscometer. The first step of overall mass transfer coefficient determination, oxygen probe was calibrated. Nitrogen was bubbled through gas sparger for the removal of dissolved oxygen from water. The oxygen probe was calibrated to 0% when the oxygen concentration was reduced to 0%. Then air was bubbled in order to increase oxygen concentration of water to 100%. At this point, the oxygen probe was calibrated to 100%. After the calibration step was completed, Nitrogen was used to strip oxygen until the oxygen concentration reduced to 0 %. Then oxygen was fed into bioreactor. The increase in dissolved oxygen concentration was recorded with respect to time. The results of three experiments were shown in appendix A.

3.4 Scale-up of 200L Bioreactor

This scale-up study was performed in this step based on the constant oxygen transfer coefficient (k_La). In maintaining a constant k_La upon scale-up from 2 to 200 L bioreactors, the agitation speed and the superficial air velocity cannot be maintained, adjustment has to be done. The Scale-up performed by firstly, investigate the k_La values in 2 L bioreactor. Next step, impeller speed was fixed and air flow rate was varied. Then, the impeller speeds and air flow rates of 200 L were determined by matching the k_La value between 2L and 200L bioreactor.

3.4.1 Geometry of 200 L bioreactor

The details of 200 L bioreactor are presented in Table 3.3. It consists of an ellipsoidal-bottom cylindrical vessel with diameter 45 cm and liquid height 80 cm and equipped with two baffles. The baffle width is 3.8 cm and 60 cm in height. The clearing space between baffle and tank bottom is 10 cm. There are three standard four blade impellers along the shaft. The impeller is 14 cm in diameter with blade height 3.2 cm. The first impeller was located at a distance of 14 cm from the bottom of vessel and the spacing between two impellers is 18 cm. Air was sparged to the tank through a ring sparger which is located at distance of 8 cm from the bottom of the bioreactor. A diameter of sparger is 10 cm with 24 holes of 1.6 mm diameter. Geometry of 200 L bioreactor and impeller was shown in Figure 3.9 and 3.10

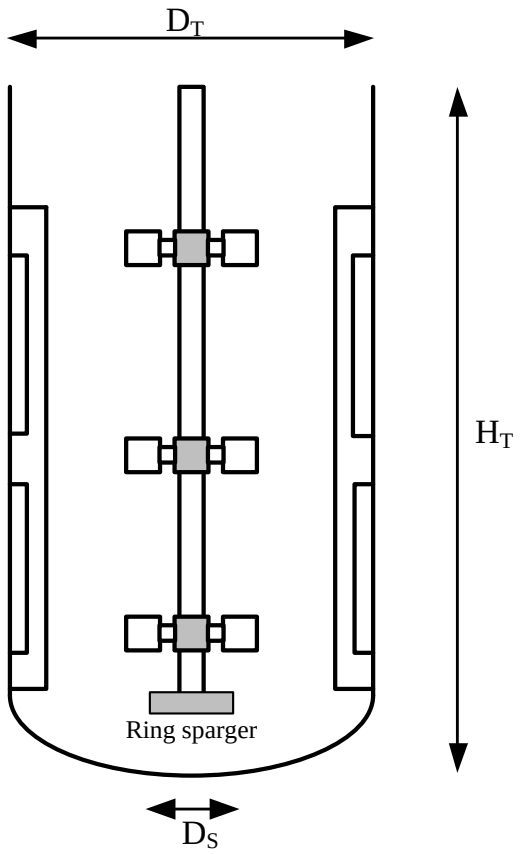

Figure 3.9 Geometry of 200 L bioreactor

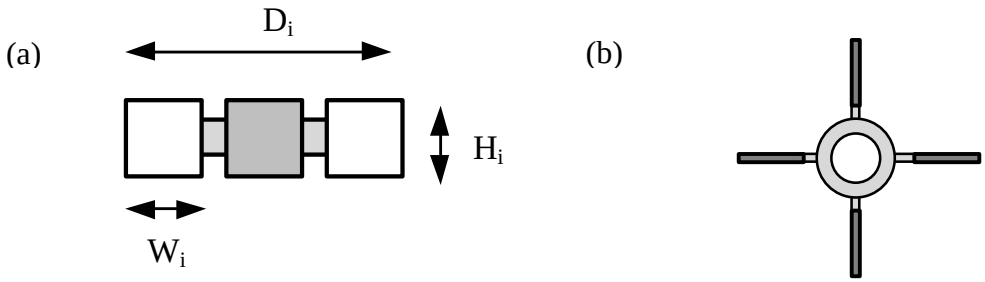

Figure 3.10 Geometry of Flat blade radial impeller of 200 L bioreactor

Table 3.3 Important dimensions of 200L bioreactor

Dimension	**2 Liter Bioreactor**
Total volume, V_T (L)	200
Working volume, V_L (L)	120
Vessel height, H_T (cm)	80
Vessel diameter, D_T (cm)	45
Impeller type	Flat blade radial impeller - 4
Number of impellers	3
Impeller diameter, D_i (cm)	13.5

Impeller thickness, T_i (cm)	0.2
Impeller width, W_i (cm)	3.5
Impeller height, H_i (cm)	3.1
Spacing between lower impeller and tank bottom (cm)	15.75
Spacing between impeller, Δ_C (cm)	25.3
Type of sparger	Ring sparger
Sparger diameter, D_S (cm)	10
Sparger distance from bottom (cm)	7.5
Number of hole	24
Hole diameter (cm)	0.2
Baffle height (cm)	60
Baffle width (cm)	3.5
Baffle thickness (cm)	0.5
Spacing between baffle and tank bottom (cm)	10
Number of baffle	2

The steps to set up CFD simulation of 200L bioreactor are the same with set up simulation of 2L bioreactor. The first step is creating the geometry of 200 L bioreactor. The solution domain was considered as only half of the vessel. One baffle was located at an angle of 90^o. Two blades of impeller were located at an angle of 45^o and 135^o. There are three impeller installed in this bioreactor. Therefore, four parts must be created which consist of one part for tank and three parts for three impellers. The geometry of tank part and impeller part were shown in Figure 3.11, 3.12 and 3.13. The second step is meshing geometry. The quality of mesh, type mesh and number of computational grid of each part were shown in the Table 3.4. The computational grid used for this simulation is shown in Fig. 3.14 and 3.15.

Table 3.4 Meshing details of each part of 200 L bioreactor

	Type of mesh	Number of element	Average quality
Tank	Hexahedral	133500	0.60
Impeller 1	Hexahedral	19390	0.63
Impeller 2	Hexahedral	19390	0.63
Impeller 3	Hexahedral	19390	0.63

(a) (b)

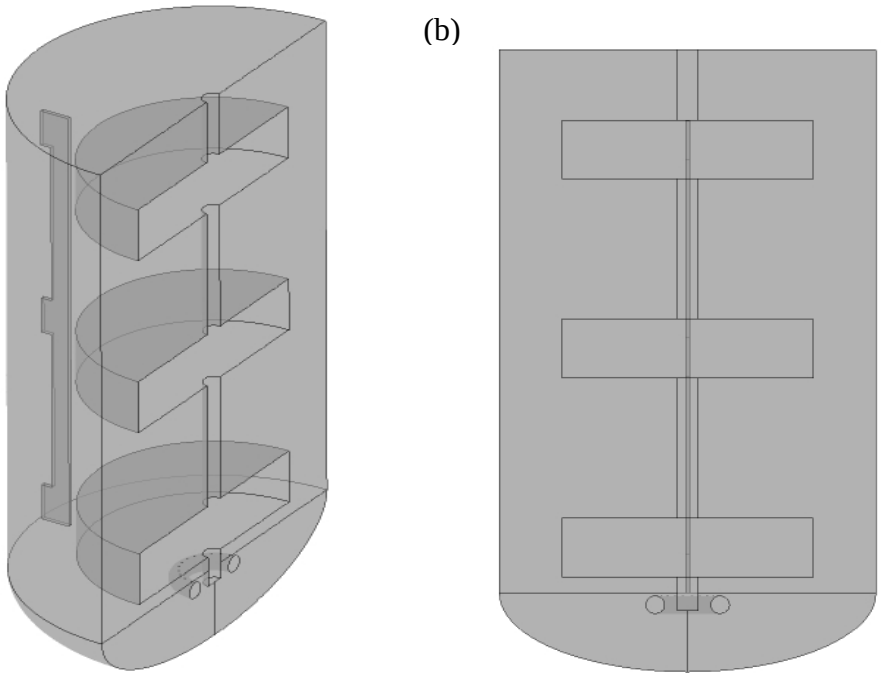

Figure 3.11 The geometry of tank part of 200 L bioreactor showed in (a) isometric view (b) front view

(a) (b)

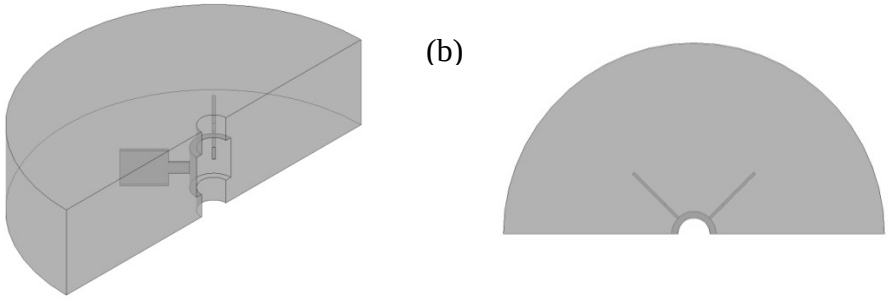

Figure 3.12 The geometry of impeller part of 200 L bioreactor showed in (a) isometric view (b) top view

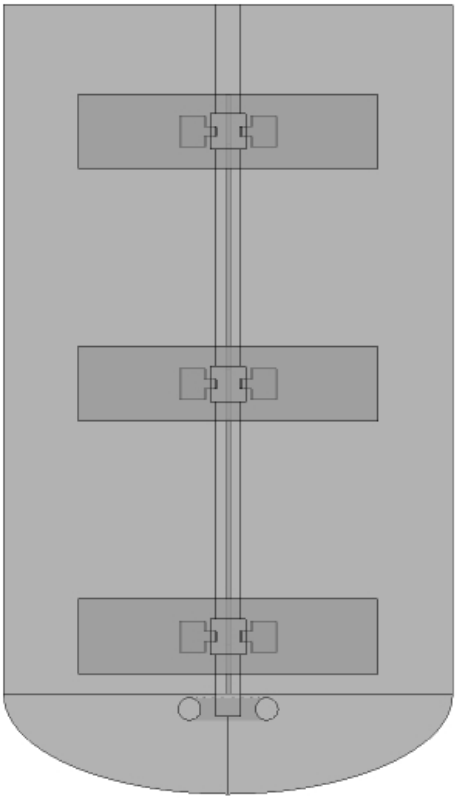

Figure 3.13 Solution domain showed in front view of 200 L bioreactor

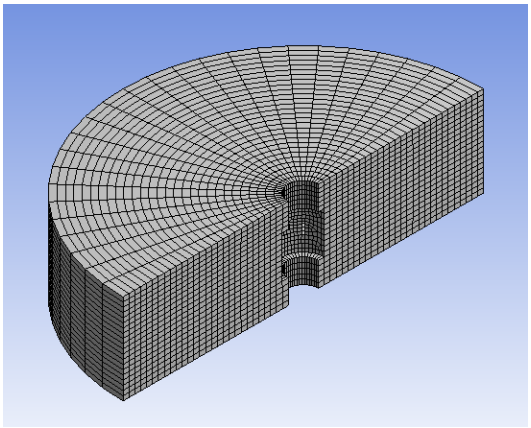

Figure 3.14 Computational gird of impeller part of 200 L bioreactor showed in isometric view

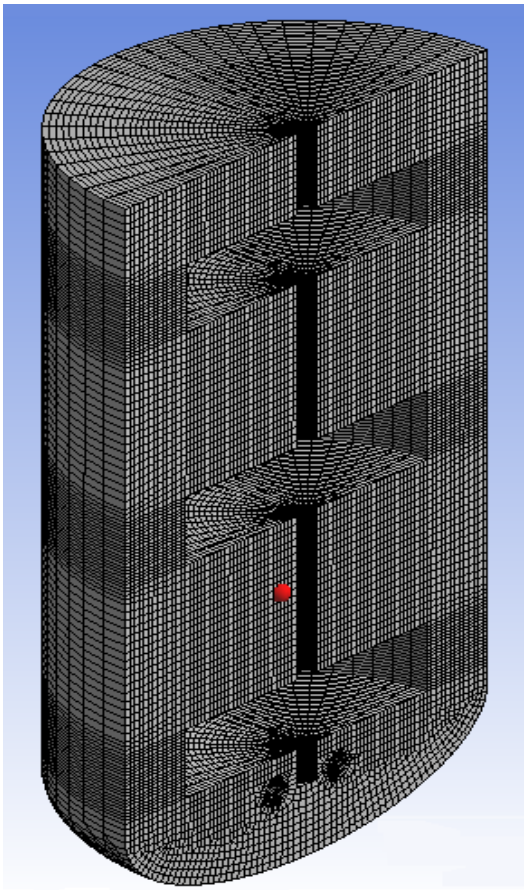

Figure 3.15 Computational gird of tank part of 200 L bioreactor showed in isometric view

3.4.2 Scale up based on constant mass transfer coefficient criterion

Scale-up fermentation processes from 2 L to 200 L bioreactor were performed with a constant oxygen transfer coefficient. In this study, the agitation speed of 200 L bioreactor was determined by the scale up equation on basis of constant power input per unit volume and constant impeller tip speed. Air feed rate was varied until the overall mass transfer coefficient of 200L bioreactor value similar with the value from 2 L bioreactor. The scale-up procedure was summarized in Figure. 3.16. This procedure applied involved the application of trial and error, interpolation and extrapolation. First, the scale-up was performed by investigate the k_La valued of 2 L bioreactor. Second, agitation speed of 200 L bioreactor was fixed and calculated by scale up equation based on constant ungassed power input per unit liquid volume (equation 2.25), gassed power input per unit liquid volume (equation 2.32) and constant impeller tip speed (equation 2.39). The scale-up equation based on constant superficial air velocity was used in order to determine the first value of air feed rate (equation 2.36). Next step, the operating agitation speed and air feed rate of 200 L bioreactor achieved from second step was used as a base line in trial – error step for scaling up on a basis of constant k_La. In the last step, air feed rate was manipulated. Interpolation and extrapolation was carried out to determine the operating variables of 200 L bioreactor.

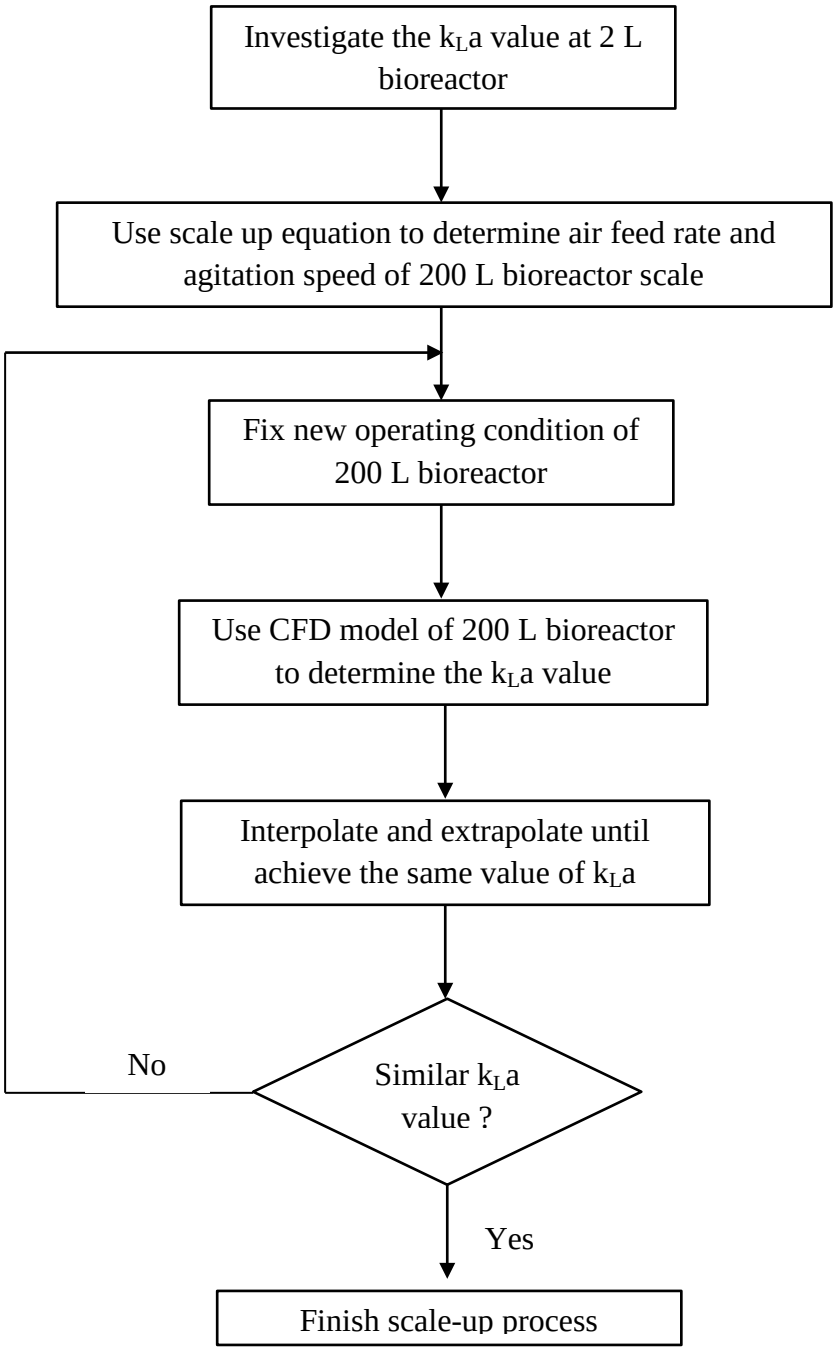

Figure 3.16 Scale up procedure based on constant overall mass transfer coefficient

CHAPTER 4 RESULTS AND DISCUSION

4.1Two phase flow simulation of 2L bioreactor

The main aim of this work is to develop the model of 2L bioreactor. Flow pattern, gas hold up, bubble size distribution and dissolved oxygen were investigated. In this research, Higbie's penetration model and Eddy model are used for the calculation of k_La. The simulation of 2L bioreactor in this step has been conducted with the same operating conditions as the experiment. The selected impeller rotational speeds in this case are 700, 800 and 900 rpm. Air flow rate is 3L/min. Liquid volume is 2L. The position of two impellers in this simulation is related to the experiment. Mass transfer coefficients predicted by numerical simulations are validated with our own experimental results.

4.1.1 Flow pattern

The flow pattern in the aerated fermenter depends on the type of impeller, geometry of impeller, clearance from the bottom, clearance above the impeller, spacing between impeller. Figure 4.1 illustrates the flow field predicted by CFD at agitation speed of 700, 800 and 900 rpm. It can be seen that the lower impeller and upper impeller generate the two ring vortices above and below the impeller disk leading to the formation of four stable rings vortices for all impellers speed. This flow pattern generated by dual Rushton turbines agitation tank system is called parallel flow and can be found in many literatures. In this pattern, the impeller discharges radial flow in which the direction was parallel with horizontal line. At the wall the water stream splits and move upward and downward along the wall before the separated streams circulate back toward the impeller.

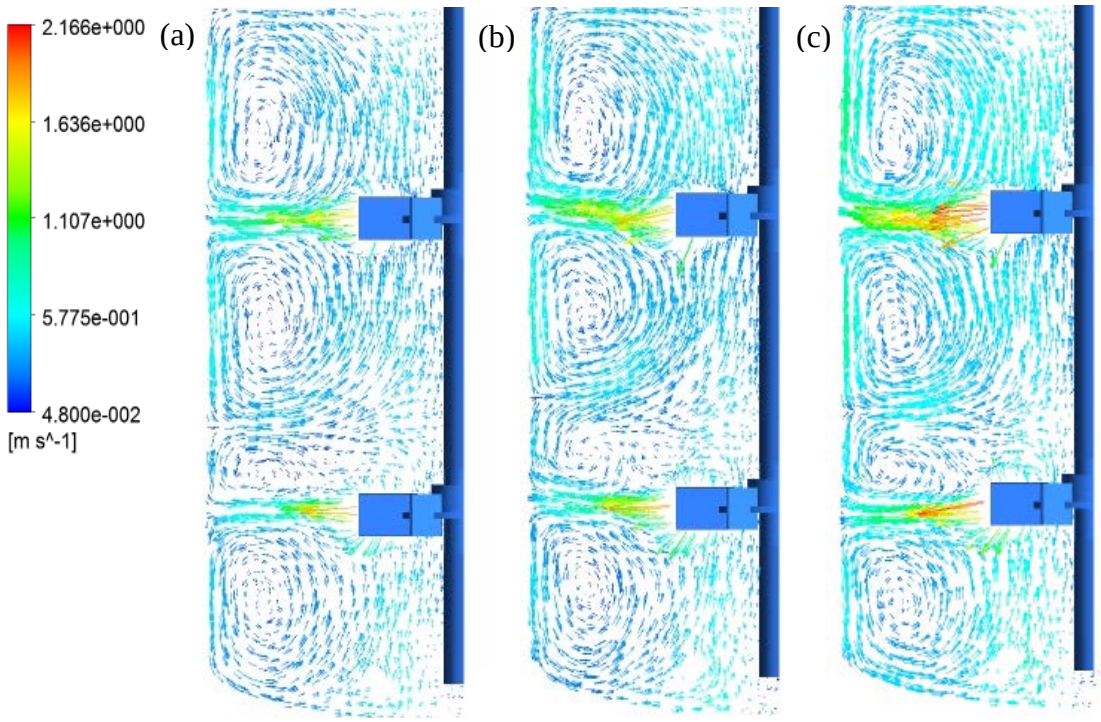

Figure 4.1 Predicted liquid phase velocity profiles in the mid plane between two baffles (a) 700 rpm (b) 800 rpm (c) 900 rpm

Figure 4.2 shows the liquid phase velocity contours at the upper impeller. The liquid phase velocity level in the bioreactor was displayed as the color rages. The red color represented high velocity while the blue color represented low velocity level. The highest velocities were found behind the impeller blades. The liquid phase velocity decreases toward the region away from the impeller discharge. The lowest water velocities were found at the tank wall. Moreover, when the impeller speed was increased, the liquid phase velocity also increases especially at the region near the impeller blades.

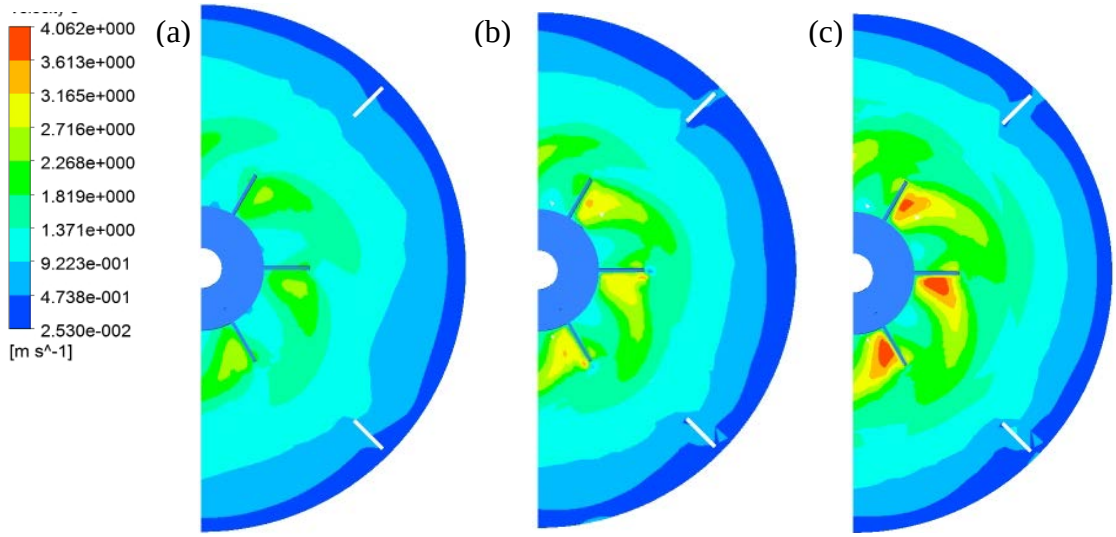

Figure 4.2 Predicted liquid phase velocity in the horizontal plane of upper impellers (a) 700 rpm (b) 800 rpm (c) 900 rpm

4.1.2 Gas hold-up

Gas hold-up is one of the most important parameters critically affecting gas liquid mass transfer rate. Gas hold up in stirred vessels is influenced by many factors but mainly by impeller speed, gas flow rate and bubble size. The gas hold up of three impeller speed showed in the mid-plane between two baffles was shown in Figure 4.3. It can be seen that gas phase is dispersed by upper impeller rather than by the lower impeller. High gas volume fraction is found around the impellers, shaft and circulating flow region. There is a large region with low gas hold-up in the region below the lower impeller. This situation indicates that the pumping capacity of the lower impeller is not sufficient to circulate gas bubbles at the bottom of the tank. The most dispersed bubbles rise directly from gas spager to lower impeller and are driven up to the upper impeller along the tank shaft. It means that the gas flow rate is too high or the impeller speed is too low leading the poorly dispersed of gas in the system.

Figure 4.4 shows the predicted contours of gas volume fraction for the lower impeller center plane. It can be seen that gas phase accumulates in the low pressure region behind the impeller blades. Only small amount of gas is dispersed by pumping force of the impeller. Accumulation of gas phase is also found around the baffles. Moreover, gas hold-up increases with an increase in agitation speed. The total gas holds up values predicted by CFD model are 3.06 % at agitation speed 700 rpm, 3.62 % at agitation speed 800 rpm and 4.6 % at agitation speed 900 rpm. This may to the fact that at higher impeller speed, the pumping capacity of impeller was enhanced leading to the large amount of oxygen induced into the liquid phase. The large bubble was also broken into

small bubble. A decrease in bubble size leads to higher gas hold-up because of the lower terminal rise velocities of smaller bubbles, leading to longer gas phase residence time.

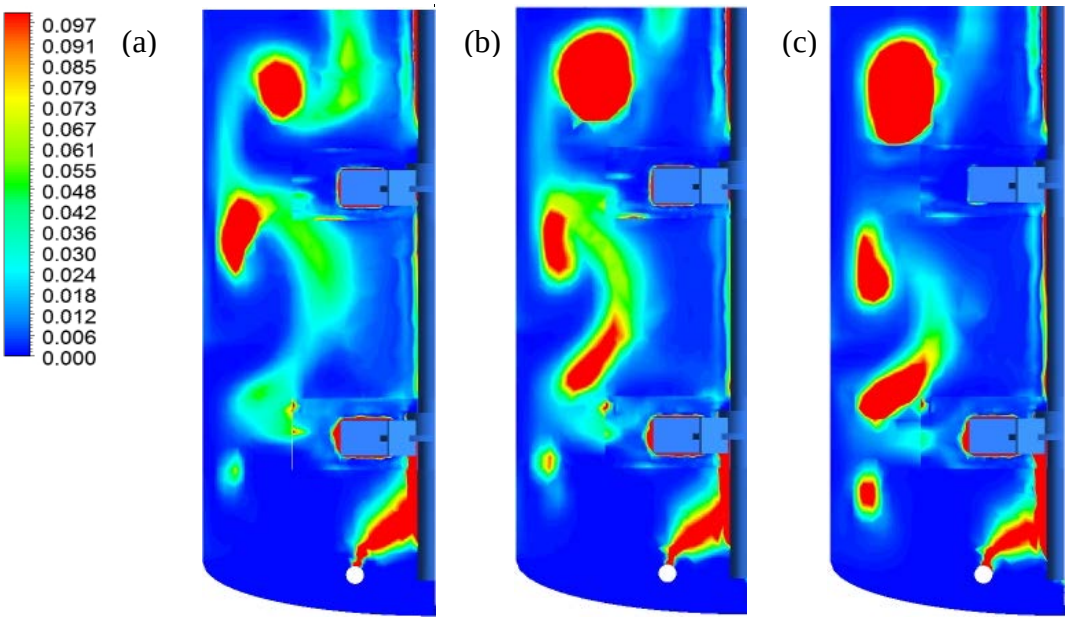

Figure 4.3 Gas hold-up in the vertical plane between the baffles (a) 700 rpm (b) 800 rpm (c) 900 rpm

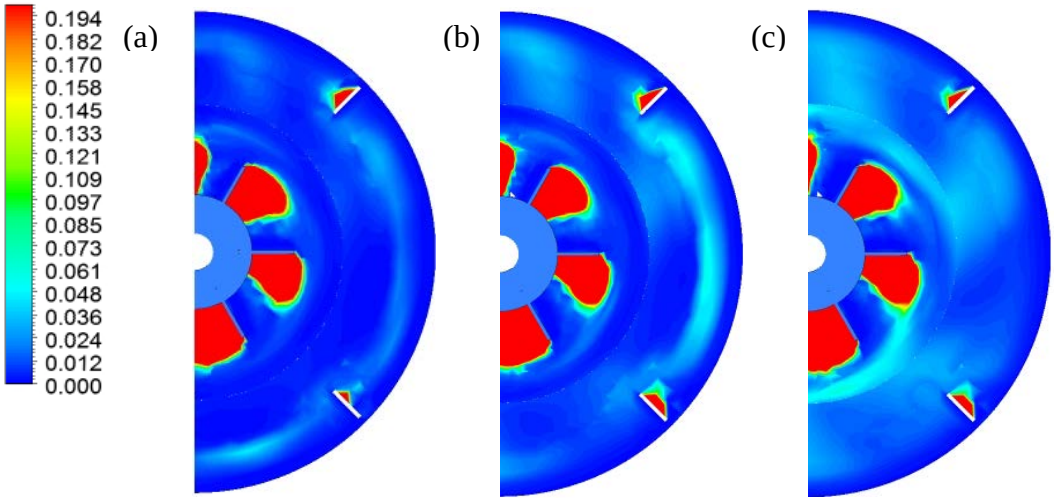

Figure 4.4 Gas hold-up in the horizontal plane at lower impeller (a) 700 rpm (b) 800 rpm (c) 900 rpm

4.1.3 Turbulent energy dissipation rate

The dissipation rate of turbulent kinetic energy is important in many mixing process. It controls the flow at micro scale and acts as a controlling parameter for many processes. For example, high turbulence energy dissipation will break up the droplet in liquid-liquid systems leading to enhance mixing efficiency. Insufficient of turbulence energy may results in poor mixing leading to more energy required to accomplish a mixing task. For the cell cultivation, shear stress can cause damage to cell due to intensive agitation in the bioreactor and reduced yield in bioreactor. Shear damage is dependent

on the local maximum energy dissipation rates [10]. Figure 4.5 shows the contour of turbulent energy dissipation rate in the vertical plane. Highest energy dissipation rate is observed in the impeller zone and in the impeller discharge stream. The values of energy dissipation rate are close to zero for the other part of tank.

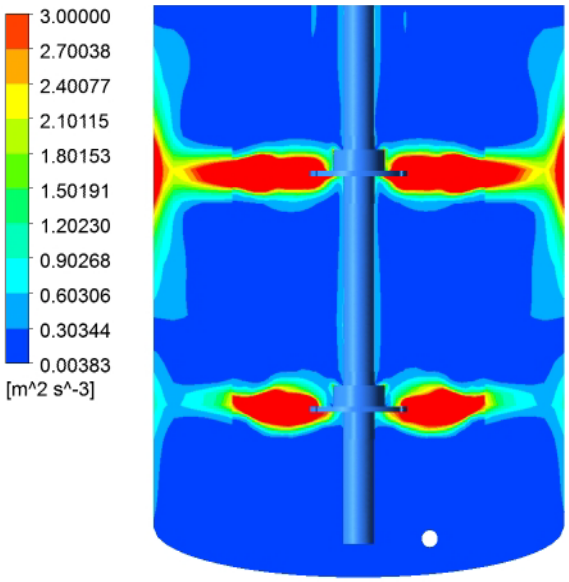

Figure 4.5 Contour of turbulence energy dissipation rate at agitation speed 700 rpm

4.1.4 Bubble size distribution

The sauter mean diameter is predicted using population balance equation function from CFX. Gas bubbles with diameters ranging from 0.5 to 10 mm are divided into 10 bubble size groups. The local size distribution of each group is show in Table 4.1.

Table 4.1 Bubble diameter of each size group used in population balance equation

Bubble group (i)	Diameter (d_i) in mm	Bubble group (i)	Diameter (d_i) in mm
1	0.97	6	5.72
2	1.92	7	6.67
3	2.87	8	7.62
4	3.82	9	8.57
5	4.77	10	9.52

Figure 4.6 shows the predicted contours of bubble size in a vertical plane between two baffles for the air flow rate of 1.5 vvm and the impeller speed of 700. It is seen that the small bubbles are found in the radial flow of lower impeller and upper impeller due to high turbulent energy dissipation rate at these regions. Bubbles are largest in the high gas fraction plume leading from the sparger to the lower impeller and also along the sharp. A high gas holdup leads to large coalescence rates because of the large number of collisions. In the region of shaft, impeller hubs and lower impeller, the turbulent energy dissipation rate is high, however, high gas volume fraction also occurs at these regions. Therefore, both coalescence and breakage of bubbles occur but coalescence prevails in these regions. Large bubbles from the coalescence are also found in the liquid circulation where the turbulent energy dissipation rate is low.

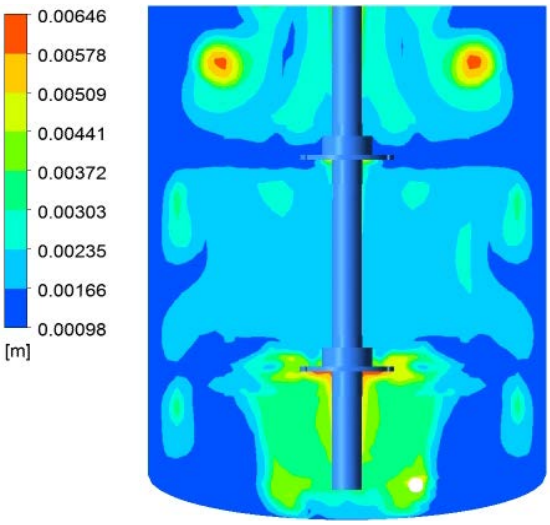

Figure 4.6 Bubble diameter in vertical plane at agitation speed 700 rpm

The distribution of gas bubble size is also presented in the horizontal plane of the lower impeller (Figure 4.7). The large bubbles are found behind the impeller blades as gas accumulates in the low pressure region. After the bubbles are pumped out by blade, they are broken up to small bubbles. It can be seen that small bubble sizes are found in the impeller discharge region. Small bubbles are generated due to break up in highly turbulent impeller discharge. Large bubbles are also found around the baffles because of the accumulation of gas phase.

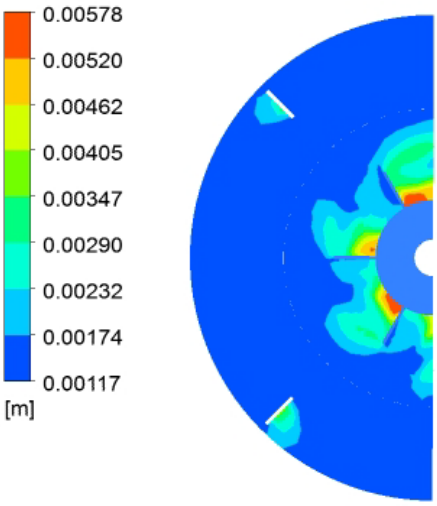

Figure 4.7 Bubble diameter of lower impeller plane at agitation speed 700 rpm

4.1.5 Mass transfer coefficient from measurement and CFD predictions

The volumetric mass transfer coefficient k_La is a very important parameter for cell cultivation. Good mass transfer performance requires large interface area between gas and liquid and a high mass transfer coefficient. For the experiment, Dissolved oxygen concentrations measured as a function of time are used in the calculating the experimental overall volumetric mass transfer coefficient (k_La). The increase in dissolve oxygen concentration is measured and recorded until the *P.patoris* media saturated with oxygen. As mentioned in the section 2.7.3, the rate of change of the dissolved oxygen concentration in liquid phase is expressed by the following equation:

$$\frac{dC_L}{dt} = k_L a(C^* - C_L) \quad (3.1)$$

Integration of Equation 3.1 with C_L=0 at t=0 leads to the following equation:

$$\ln\left(\frac{C^* - C_L}{C^*}\right) = -k_L a.\, t \quad (3.2)$$

Plotting of the Ln term against time gives the experimental overall volumetric mass transfer coefficient. The raw data of all experiments was analyzed and shown in the appendix A. Overall mass transfer coefficient of all experiments was shown in the Table 4.2. The $k_L a$ values increased from 75.24 to 132.12 hr^{-1} as the agitation speed was increased from 700 to 900 rpm with the same air feed rate.

Using the CFD simulation, the volumetric mass transfer coefficient is calculated by penetration model and eddy cell model. The contours of local mass transfer coefficient (k_L) predicted from both models at agitation speed 700 rpm were shown in Figure 4.8. The local mass transfer obtained from both models show higher values at the impellers discharge region and the lower values at the bulk region. For this reason, the mass transfer coefficients calculated from these models depend on the turbulent energy dissipation rate which is high in the both impellers discharge region and lower in the other part of vessel. When comparing results from two models, the predicted local mass transfer coefficient from penetration model is higher than the predicted local mass transfer coefficient from eddy cell model.

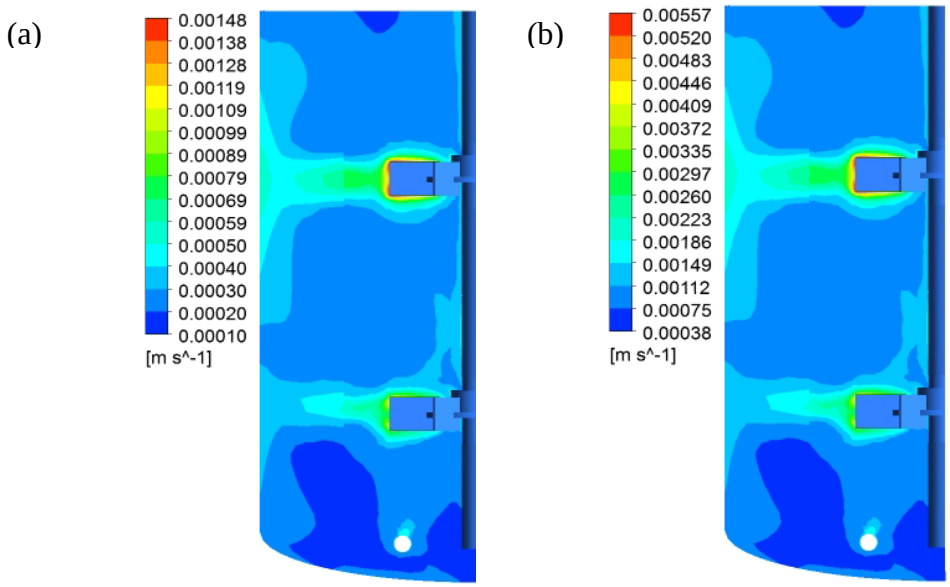

Figure 4.8 Contours of local mass transfer coefficient (k_L) at agitation speed 700 rpm predicted from (a) Eddy cell model (b) penetration model

Figure 4.9 shows the predicted overall mass transfer coefficient ($k_L a$). It is calculated as the product of local mass transfer coefficient and interfacial area. Therefore, High $k_L a$ values are expected in the high gas hold up and high turbulence energy dissipation rate regions. It can be seen that overall mass transfer coefficient reached maximum at the impeller discharge region and around the tank shaft. The overall mass transfer coefficient is low at the other part of tank although there is a large interfacial available. This is because the mass transfer coefficient is assumed to depend on the turbulent

dissipation rate, which is small at all part of tank except the impeller discharge region. In order to get high mass transfer rate, both turbulence energy dissipation rate and large mass transfer area are required to be located at the same location which is found only the region around shaft, impeller blades and out flow of both impellers

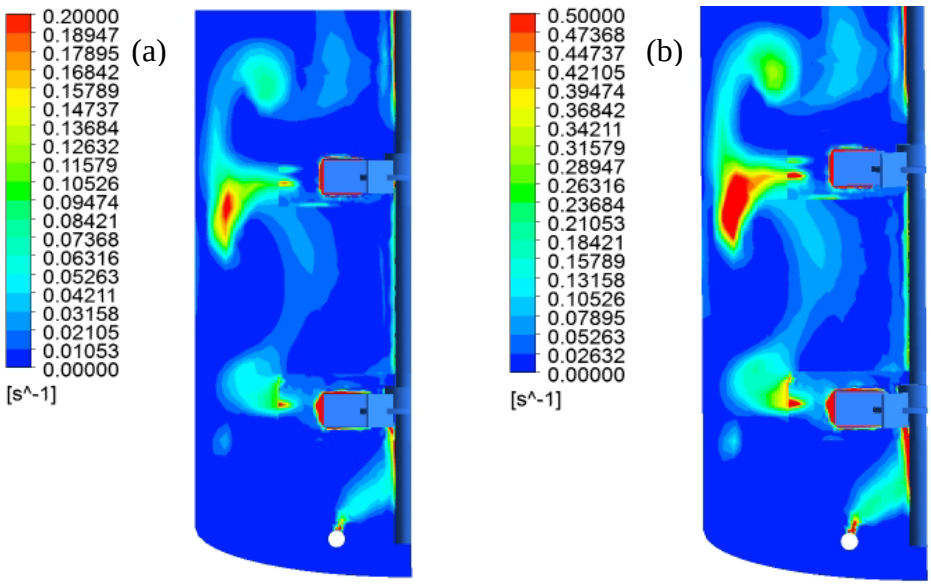

Figure 4.9 Contours of overall mass transfer coefficient (k_La) at agitation speed 700 rpm predicted from (a) Eddy cell model (b) penetration model

The volume averaged overall mass transfer coefficients predicted from penetration and eddy cell model along with experimental results are show in the Table 4.2. It can be seen that the predicated overall mass transfer coefficients are different for different mass transfer models. The predicted mass transfer coefficient from both penetration model and eddy cell model give the higher values compared to the experimental results at all agitation speed. The predicted mass transfer coefficient is very much higher for penetration model. It can be concluded that predicted mass transfer coefficient from eddy cell model match very well with experimental results. It is also seen that mass transfer coefficient increases with an increase of agitation speed.

Table 4.2 Overall mass transfer coefficient obtained from CFD simulation and experiment.

Agitation speed (rpm)	**Overall mass transfer coefficient (k_La)**		
	Experimental (hr^{-1})	**Penetration (hr^{-1})**	**Eddy cell (hr^{-1})**
700	75.24	325.80	78.29
800	102.60	502.92	115.16
900	132.12	657.00	148.34

4.1.6 Prediction of Dissolved oxygen

In this step, oxygen concentration in liquid phase was calculated using mass transfer coefficient from eddy cell model. Dissolved oxygen was specified as addition scalar variable. The transport equation was defined in order to predict the dissolved oxygen in

the bioreactor. The general transport equations of scalar variable in multiphase flow are expressed as

$$\frac{\partial}{\partial t}(r_\alpha \emptyset_\alpha) + \nabla.(r_\alpha \emptyset_\alpha v_\alpha) - \nabla.[r_\alpha(J_\alpha + \emptyset'_\alpha v'_\alpha)] = L_\alpha \quad (3.3)$$

L_α represents the interfacial transfer of concentration. J_α is the flux due to molecular diffusion. $\emptyset'_\alpha v'_\alpha$ represents the flux due to the turbulent diffusion of the concentration. The oxygen mass transfer from gas phase to liquid phase was modeled using two-film theory and was expressed by the following equation

$$L_\alpha = k_L a(\emptyset_l^* - \emptyset_l) \quad (3.4)$$

$\emptyset_l^*$ is the saturation concentration of oxygen in liquid phase. In this work, $\emptyset_l^*$ in media culture was assumed to be equal with the water system and was calculated according to Henry's law. The local mass transfer coefficient calculated from eddy cell model was selected because local mass transfer predicted from this model matches very well with experimental result. Oxygen uptake rate of the cells in the bioreactor was set as equal to 2.37 x 10^{-4} kg/m^{3}s. This value was obtained from the experimental results of Baumann *et al* [26]. The details of the calculation of dissolved oxygen and oxygen uptake rate by cell were shown in Appendix B. The initial value of dissolved oxygen in the bioreactor was specified by using the equation that was a function of pressure.

The contour plot of dissolved oxygen at agitation speed 900 rpm was shown in Figure 4.10. The red color represented the high value of dissolved oxygen whereas the blue color represented the low value of dissolved oxygen. It can be observed that the dissolved oxygen concentration shows the high value at the impellers discharge region, along the shaft and circulating flow region because the oxygen transfer rate was high at these regions. The low dissolved oxygen concentration was observed in the regions with poor gas distribution which is the region below the tank shaft. The average dissolved oxygen values predicted from CFD at agitation speed 700, 800 and 900 rpm were shown in the Table 4.3. It can be observed that the value of dissolved oxygen concentration is highest at agitation speed 900 rpm. It was because the predicted overall mass transfer coefficient in this case is higher than the other cases. Larger $k_L a$ value means the higher the aeration capacity of the system. It was also observed that the average dissolved oxygen from case 1 and case 2 is reported in negative value. It means that the amount of oxygen in the bioreactor is not enough for microorganism consumption at rate 2.37 x 10^{-4} kg/m^{3}s. Therefore, the operation condition in case 1 and case 2 is not suitable for cell cultivation. The oxygen concentration should be enhanced about 5.011g/m^3 and 0.549 g/m^3 for support the oxygen consumption by cell.

Table 4.3 The average dissolved oxygen in the bioreactor from three agitation speeds

Parameter	Unit	Case 1	Case 2	Case 3
Agitation speed	rpm	700	800	900
Flow rate of air inlet	L/min	3	3	3
Overall mass transfer coefficient predicted from eddy cell model	(hr^{-1})	78.29	115.16	148.34
Calculated oxygen concentration from CFD	g/m^3	-5.011	-0.549	1.465

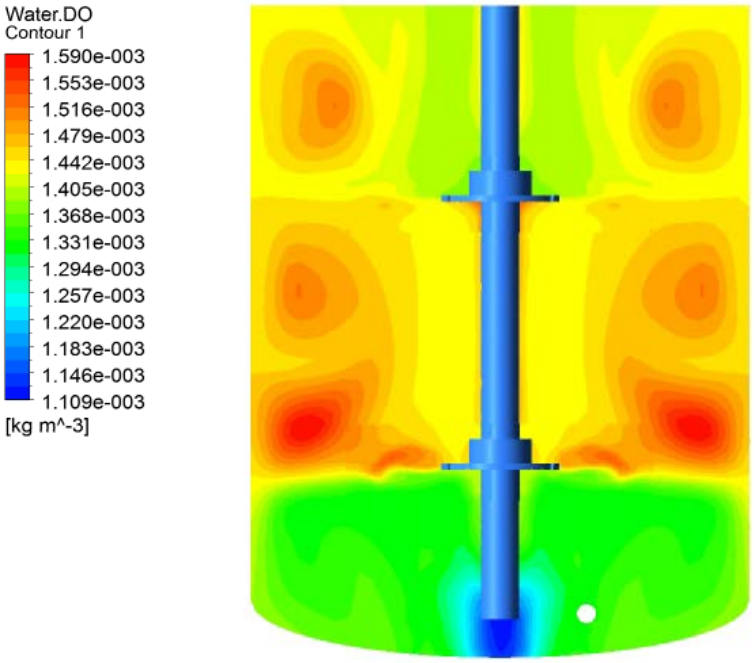

Figure 4.10 Contour plot of dissolved oxygen concentration by CFD simulation with eddy cell model at agitation speed 900 rpm

4.2 Scale-up on a basis of constant k_La from 2 L to 200 L bioreactor

4.2.1 Determination of Operating Variables at 200 L bioreactor

The scale-up equations was applied in order to determine the initial value of the operating variables of 200 L bioreactor. Working volume of liquid using for simulation is 120L. The air feed rate was calculated using scale-up equation based on constant gas superficial velocity. Then, the impeller speed was calculated using scale-up equation based on constant ungassed power consumption per unit liquid volume, gassed power consumption per unit liquid volume and constant impeller tip speed. The results for the determination of air flow rate and impeller speeds at 200 liter scale bioreactor were shown in Table 4.4.

Table 4.4 Determination of air feed rate and agitation speed at 200 L bioreactor scale

Bioreactor scale	Air feed rate (L/min)	Agitation speed (rpm)		
	Constant air superficial velocity	Constant P_o/V	Constant P_g/V	Constant impeller tip speed
2 L (base case)	3	900	900	900
200 L (scale up)	36	480	470	350

The operating variables at 200 L scale bioreactor obtained from Table 4.4 cannot be adopted directly in order to achieve a similar k_La value between 2 L bioreactor and 200 L bioreactor. The results obtained from scale-up equation were used as an initial value of the operating impeller speed and air flow rate. In order to achieve the similar k_La value at 200 L bioreactor scale, the impeller speed of 200 L bioreactor obtained from

Table 4.4 was fixed and air feed rate was varied. In case of agitation speed obtained from scale up equation based on constant P_o/V, the agitation speed of 200 L bioreactor was fixed at 480 rpm. In case of agitation speed obtained from scale up equation based on constant P_g/V, the agitation speed of 200 L bioreactor was fixed at 470 rpm. In case of agitation speed obtained from scale up equation based on impeller tip speed, the agitation speed of 200 L bioreactor was fixed at 350 rpm. The initial air feed rate is 36 L/min for all cases.

4.2.2 Operating agitation speed and air feed rate of 200L bioreactor on a basis of constant k_La

The result from scale up procedure based on constant mass transfer coefficient was shown in Table 4.5a, 4.5b and 4.5c. From Table 4.5a and 4.5c, it can be seen that scale-up procedure base on constant k_La criteria was successfully employed in this study to find the operation variables at 200 L bioreactor scale. The similar k_La value between 2 L bioreactor and 200 L bioreactor was obtained at third iteration in case of agitation speed obtained from scale up equation based on constant P_o/V and first iteration in case of agitation speed obtained from scale up equation based on constant P_g/V. In conclusion, the new operating agitation speed of 200L bioreactor scale is 480 rpm which was obtained from scale up equation based on constant P_o/V and the operating air feed rate is about 16.43 L/min or 0.14 vvm. In case of agitation speed obtained from scale up equation based on constant P_g/V, the new operation conditions of 200 L bioreactor are agitation speed 470 rpm and air feed rate 0.3 vvm.

From Table 4.5c, it can be seen that at agitation speed of 350 rpm, increasing in air feed rate cannot enhanced the mass transfer coefficient reached to the design value. After increase air feed rate from 85.78 L/min to 120 L/min, the mass transfer coefficient remain constant. This is because the impeller speed of 200L bioreactor scale was calculated for scale up equation based on constant impeller speed. If scale up is conducted using constant impeller tip speed, the value of P/V is lowered which can adversely affect aeration efficiency. Reduction in the power input per unit volume results in reduction of the rate of oxygen transport [25]. It can be also seen that the mass transfer coefficient decrease when air feed rate was increased from 120 L/min to 160 L/min. It means that the gas flow rate is too high leading to poor dispersion of gas phase in the system. The pumping capacity of the impeller is not sufficient to disperse a gas phase. This phenomenon is called flooding. The flooding phenomenon occurs when the power input by agitation speed is too low to disperse a gas phase. Gas dispersion becomes inefficient. This phenomenon is an undesirable condition and can be avoided by decreasing the gas flow rate for a given stirrer speed or by increasing the stirrer speed for a given gas flow rate. In conclusion, using scale up equation based on constant impeller speed to calculate the impeller speed is not suitable for determine the new operation condition of 200L bioreactor scale. The impeller speed of 200 bioreactor scale obtained from this equation is too low to maintain a constant mass transfer coefficient during the scaling up bioreactor.

Table 4.5 Result from scale up procedure based on constant mass transfer coefficient

(a) Agitation speed obtained from scale up equation based on constant P_o/V

2 L bioreactor			200 L bioreactor				
Agitation speed (rpm)	**Air feed rate (L/min)**	**k_La (hr^{-1})**	**No.**	**Agitation speed (rpm)**	**Air feed rate (L/min)**	**Air feed rate (vvm)**	**k_La (hr^{-1})**
900	3	148.32	1	480	36	0.30	159.48
			2	480	33.48	0.28	158.04
			3	480	16.43	0.14	146.48

(b) Agitation speed obtained from scale up equation based on constant P_g/V

2 L bioreactor			200 L bioreactor				
Agitation speed (rpm)	**Air feed rate (L/min)**	**k_La (hr^{-1})**	**No.**	**Agitation speed (rpm)**	**Air feed rate (L/min)**	**Air feed rate (vvm)**	**k_La (hr^{-1})**
900	3	148.32	1	470	36	0.30	151.16

(c) Agitation speed obtained from scale up equation based on constant impeller tip speed.

2 L bioreactor			200 L bioreactor				
Agitation speed (rpm)	**Air feed rate (L/min)**	**k_La (hr^{-1})**	**No.**	**Agitation speed (rpm)**	**Air feed rate (L/min)**	**Air feed rate (vvm)**	**k_La (hr^{-1})**
900	3	148.32	1	350	36	0.30	62.24
			2	350	85.78	0.71	85.39
			3	350	120	1.00	86.41
			4	350	160	1.33	81.90

CHAPTER 5 CONCLUSIONS AND RECOMENDASIONS

5.1 Conclusions

A CFD model of gas liquid dispersion in a stirred bioreactor coupled with population balance equations was developed in order to study the hydrodynamic and predict the mass transfer in a 2 L laboratory scale bioreactor. A steady state method of multiple frame of reference was used to model the impeller and tank regions. Mass transfer coefficient was calculated based on Higbie's penetration theory and Eddy cell model. Flow pattern, gas hold up, Sauter mean bubble diameter and turbulence energy dissipation rate were captured from CFD analysis. The experimental determinations of mass transfer coefficient were performed to validate the CFD model. The predicted mass transfer coefficient from CFD model was compared with the experimental results. From the results, it was observed that the mass transfer coefficient calculated from eddy cell model closely matches with the experimental result while the mass transfer coefficient calculated from Higbie's penetration theory shows the higher value than the experiment results. Gas hold up, liquid phase velocity, mass transfer coefficient and dissolved oxygen increase with an increase in agitation speed. The model presented in this paper will be useful for finding the best operating conditions of 2 L laboratory scale bioreactor.

After the CFD model of 2 L bioreactor was successfully developed, the scale-up of the bioreactor from 2 L scale to 200 L scale was performed based on constant mass transfer coefficient criteria. The scale up procedure based on constant mass transfer coefficient was proposed in this study. The agitation speed of 200 L bioreactor was calculated using scale up equation based on constant power consumption per unit liquid volume and constant impeller tip speed. Air feed rate was manipulated in order to get the similar mass transfer coefficient value between 2 L bioreactor and 200 L bioreactor. From the results, scale up procedure with agitation speed obtained from scale up equations based on constant ungassed power input per unit volume and gassed power input per unit volume were successfully employed in this study. On the other hand, the scale up equation based on constant impeller tip speed used for calculation the impeller speed of 200 L bioreactor scale was not suitable for the scaling up bioreactor on the basis of constant mass transfer coefficient.

5.2 Recommendations

5.2.1 The validation of CFD model of 200 L bioreactor should be performed in order to investigate the accuracy of the results from model.

5.2.2 The scale up procedure proposed in this work based on the constant mass transfer coefficient criteria. Other scale-up criteria such as constant dissolved oxygen, constant shear stress should be performed in scaling up bioreactor.

REFERENCES

1. Xu Wang, Jie Ding , Wan-Qian Guo and Nan-Qi Ren, 2010, "A hydrodynamics-reaction kinetics coupled model for evaluating bioreactors derived from CFD simulation", **Bioresource Technology**, Vol. 101, Issue 24, pp. 9749-9757.

2. M.R. Bhole, J.B. Joshi and D. Ramkrishna, 2008, "CFD simulation of bubble columns incorporating population balance modeling", Chemical Engineering Science, Vol. 63, pp. 2267 – 2282.

3. Ghasem D. Najafpour, 2007, "**Biochemical Engineering and Biotechnology**", Elsevier's Science & Technology, pp.228-230.

4. Wei Zhang, Zheng Jian Li, Foster and A. Agblevor, 2005, "Microbubble fermentation of recombinant *Pichia pastoris* for human serum albumin production", **Process Biochemistry,** Vol.40, Issue 6, pp. 2073-2078**.**

5. S. Sivaprakasam, S. Mahadevan and S. Gopalaraman, 2008, "Oxygen mass transfer studies on batch cultivation of P. aeruginosa in a biocalorimeter", **Electronic Journal of Biotechnology,** Vol.11, Issue 1.

6. Kumar M. Dhanasekharan, Jay Sanyal, Anupam Jain and Ahmad Haidari, 2005, "A generalized approach to model oxygen transfer in bioreactors using population balances and computational fluid dynamics", **Chemical Engineering Science,** Vol.60, pp.213-218.

7. F. Kerdouss,A. Bannari and P. Proulx, 2006, "CFD modeling of gas dispersion and bubble size in a double turbine stirred tank", **Chemical Engineering Science,** Vol.61, pp.3313-3322.

8. Jian Min, Yuyun Bao, Lei Chen, Zhengming Gao, and John M. Smith, 2008, "Numerical simulation of gas dispersion in an aerated stirred reactor with multiple impellers", **Industrial & Engineering Chemistry Research,** Vol.47, pp. 7112-7117.

9. P. Ranganathana and S. Sivaraman, 2008, "Investigations on hydrodynamics and mass transfer in gas-liquid stirred reactor using computational fluid dynamics", **Chemical Engineering Science**.

10. Hu Zhang, Kai Zhang and Shengdi Fan, 2009, "CFD simulation coupled with population balance equations for aerated stirred bioreactors", **Engineering in Life Sciences**, Vol.9, No.6, pp. 421-430.

11. Vijaya Krishna Bodla., **"**Evaluation of the Scale-up potential of the mammalian cell fermenters within NovoNordisk**"**, **Master of Special Research Project, Master of Science in Chemical Engineering**, Denmarks Technical University, p.7.

12. M. Jahoda, L. Tomaskova and M. Mostek, 2009, "CFD prediction of liquid homogenisation in a gas-liquid stirred tank", **Chemical Engineering Research and Design**, Vol.87, pp. 460-467.

13. J. Gimbun, C. D. Rielly and Z. K. Nagy, 2009, "Modelling of Mass Transfer in Gas-Liquid Stirred Tanks Agitated by Rushton Turbine and CD-6 Impeller", **European Conference on Mixing**, 14-17 April 2009, London, p. 1.

14. K. Rutherford, K. C. Lee, S. M. S. Mahmoudi and M. Yianneskis, 1996, "Hydrodynamic Characteristics of Dual Rushton Impeller Stirred Vessels", **The American Institute of Chemical Engineers,** Vol. 42, No. 2.

15. ANSYS Technology, **CFX-13 user Manual**, 2010, Harwell, United Kingdom

16. Pasi Moilanen., **"Modeling gas-liquid flow and local mass transfer in stirred tanks"**, Master of Special Research Project, Doctor of Science in Technology, Helsinki University of Technology, p.23.

17. M. Zadravec*, S. Basic, M. Hribersek, 2007, "The influence of rotating domain size in a rotating frame of reference approach for simulation of rotating impeller in a mixing vessel", **Journal of Engineering Science and Technology**, Vol. 2, No. 2.

18. H.K. Lim, S.J. Choi, K.Y. Kim and K.H. Jung, 2003, "Dissolved-oxygen-stat controlling two variables for methanol induction of rGuamerin in *Pichia pastoris* and its application to repeated fed-batch", **Applied Microbiology and Biotechnology**, Vol.62, pp. 342-348.

19. Mariano Martín, Francisco J. Montes and Miguel A. Galán, 2003, "Bubbling process in stirred tank reactors I: Agitator effect on bubble size, formation and rising", **Chemical Engineering Science**, Vol.63, pp. 3212-3222.

20. Gabriel Potvin, Ayla Ahmad and Zisheng Zhang, "Bioprocess engineering aspects of heterologous protein production in *Pichia pastoris*: A review", **Biochemical Engineering Journal**.

21. Felix Garcia-Ochoa and Emilio Gomez, 2004, "Theoretical prediction of gas–liquid mass transfer coefficient, specific area and hold-up in sparged stirred tanks", **Chemical Engineering Science**, Vol.59, pp. 2489-2501.

22. Pauline M. Doran, 1995, "Biochemical Engineering and Biotechnology", **Elsevier Science & Technology Books**, p195.

23. Michael Sulu, 2009, "The Process Intensification of Biological Hydrogen Production by *Escherichia coli* HD701", **A thesis submitted for the degree of DOCTOR OF PHILOSOPHY**, The University of Birmingham.

24. Felix Garcia-Ochoa and Emilio Gomez, 2009, "Bioreactor scale-up and oxygen transfer rate in microbial processes: An overview", **Biotechnology Advances**, Vol.27, pp. 153-176.

25. Beth Helene Junker, 2004, "Scale-up methodologies for *Escherichia coli* and yeast fermentation processes", **Journal of Bioscience and Bioengineering,** Vol. 97, Issue 6, pp. 347–364.

26. Baumann K, Maurer M, Dragosits M, Cos O, Ferrer P, Mattanovich D, 2008, “Hypoxic fed-batch cultivation of Pichia pastoris increases specific and volumetric productivity of recombinant proteins” , **Biotechnology and Bioengineering,** Volume 100, Issue 1, pp. 177–183

Appendix A

The experiments for Overall Mass transfer coefficient determination

A.1 Overall mass transfer coefficient calculation of experiment at agitation speed 700 rpm and air feed rate 3L/min

Table A.1 The Data obtained from experiment at agitation speed 700 rpm and air feed rate 3L/min

Time (sec)	C_a	Ln term
10	0	0.000
20	0.1	0.001
30	1	0.010
40	8.4	0.088
50	17.8	0.196
60	26.9	0.313
70	35.9	0.445
80	44.2	0.583
90	51.4	0.722
100	58	0.868
110	64.6	1.038
120	70.9	1.234
130	76.4	1.444
140	81.4	1.682
150	86	1.966
160	90	2.303
170	93.5	2.733
180	95.6	3.124
190	96.9	3.474
200	97.4	3.650
210	97.9	3.863
220	98.3	4.075

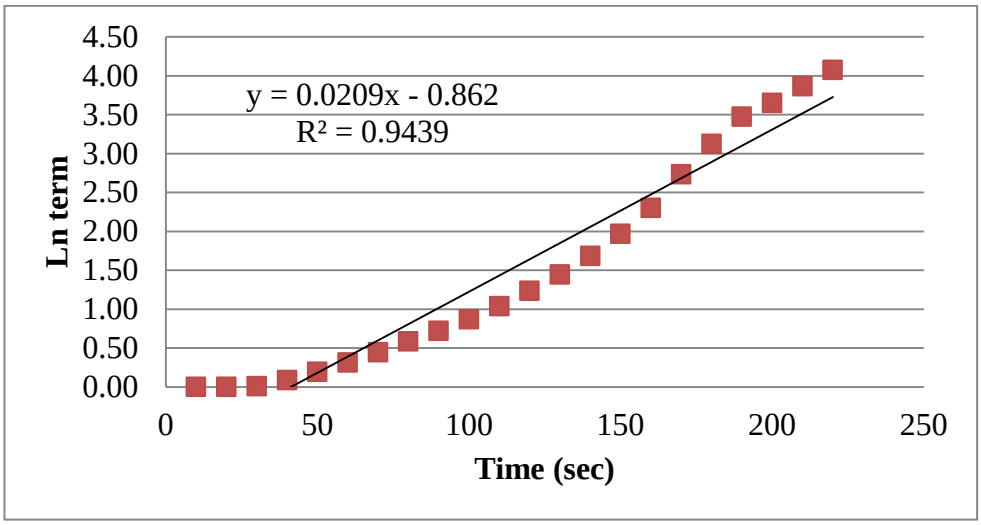

Figure A.1 The graph shows relationship between Ln term and Time at agitation speed 700 rpm and air feed rate 3L/min

The slope of graph is equal to 0.0209. Therefore, the overall mass transfer coefficient (k_La) obtained from experiment at agitation speed 700 rpm and air feed rate 3L/min is 0.0209 s^{-1}.

A.2 Overall mass transfer coefficient calculation of experiment at agitation speed 800 rpm and air feed rate 3L/min

Table A.2 The Data obtained from experiment at agitation speed 800 rpm and air feed rate 3L/min

Time (sec)	C_a	Ln term
10	0.7	0.007
20	6.3	0.065
30	16	0.174
40	28.2	0.331
50	41.5	0.536
60	56.1	0.823
70	68.4	1.152
80	76.7	1.457
90	83.3	1.790
100	88.8	2.189
110	92.1	2.538
120	94.3	2.865
130	96.2	3.270
140	97	3.507
150	97.5	3.689
160	97.9	3.863
170	98.3	4.075
180	98.8	4.423

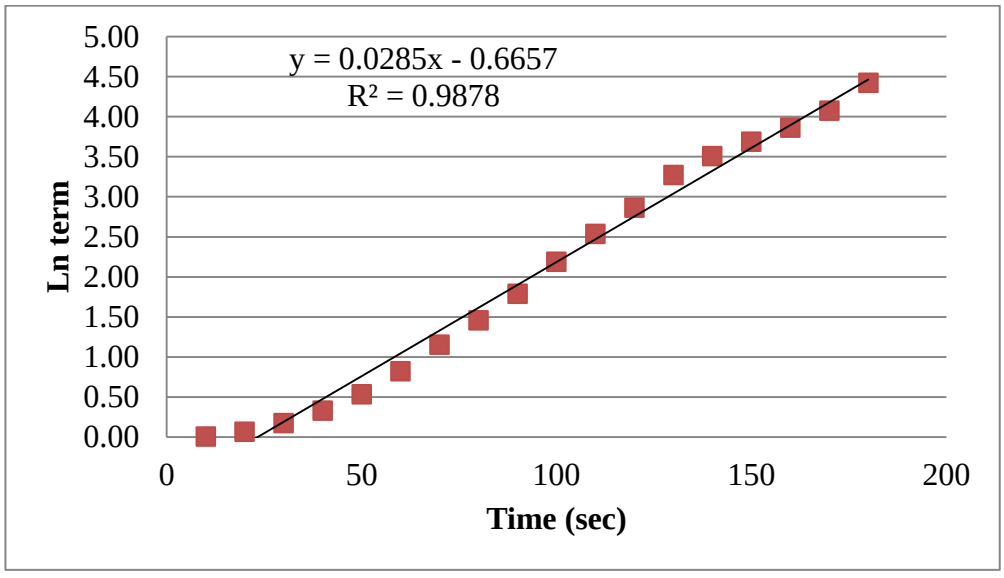

Figure A.2 The graph shows relationship between Ln term and Time at agitation speed 800 rpm and air feed rate 3L/min

The slope of graph is equal to 0.0285. Therefore, the overall mass transfer coefficient (k_La) obtained from experiment at agitation speed 800 rpm and air feed rate 3L/min is 0.0285 s^{-1}.

A.3 Overall mass transfer coefficient calculation of experiment at agitation speed 900 rpm and air feed rate 3L/min

Table A.3 The Data obtained from experiment at agitation speed 900 rpm and air feed rate 3L/min

Time (sec)	Ca	Ln term
10	0.8	0.008
20	7.4	0.076
30	18.5	0.204
40	31.6	0.379
50	45.2	0.601
60	58.5	0.879
70	71.9	1.269
80	83.6	1.807
90	89.2	2.225
100	94.5	2.900
110	96.3	3.296
120	97.4	3.649
130	98.4	4.135

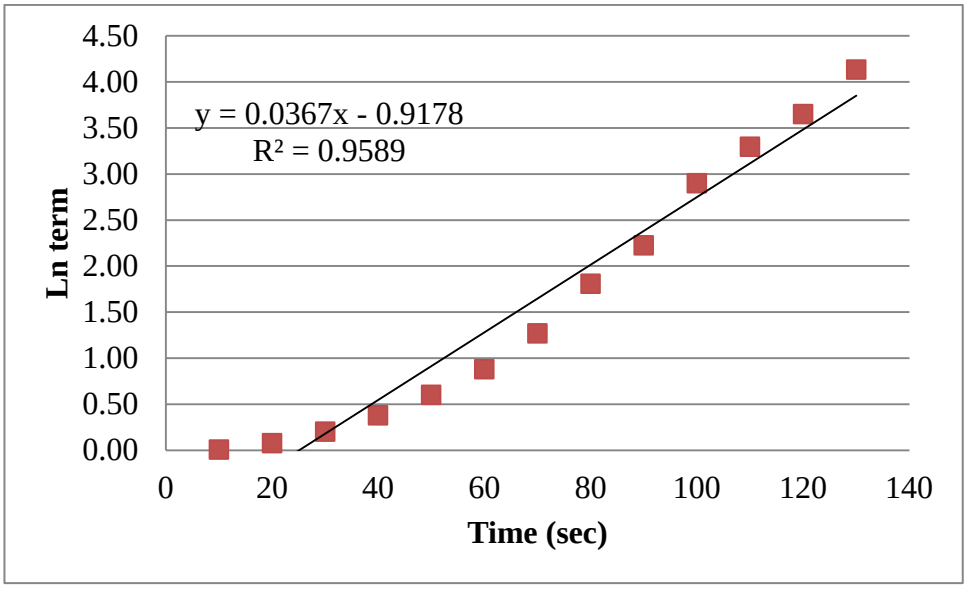

Figure A.3 The graph shows relationship between Ln term and Time at agitation speed 900 rpm and air feed rate 3L/min

The slope of graph is equal to 0.0367. Therefore, the overall mass transfer coefficient (k_La) obtained from experiment at agitation speed 800 rpm and air feed rate 3L/min is 0.0367 s^{-1}.

Appendix B

The calculation of oxygen uptake rate by cell and oxygen solubility

B.1 The calculation of oxygen uptake rate by cell in chemostat cultivation condition

The Oxygen uptake rate (OUR) by cell used in this research came from the experimental results of Baumann et al. [26].
Oxygen uptake rate of *P.pastoris* in chemostat condition = 2.23 mmol /g_{YDM} h
The cell dry mass concentration = 11.99 g/L

$\therefore$ Total Oxygen up take rate by cell = 11.99 g/L x 2.23 mmol /g_{YDM} h
= 26.7377 mmol/ h.L
= 2.3765 x 10^{-4} kg/m^3.s

B.2 The calculation of oxygen solubility in water

The saturation oxygen concentration in an air-liquid system is calculated by Henry's law, which can be written as:

$$C_L^* = \frac{y_g P_g}{He}$$

where ; C_L^* = saturation oxygen concentration of liquid phase
y_g = mole fraction of oxygen in gas phase
P_g = total pressure of gas phase
He = Henry's constant

Example – Calculating saturation oxygen concentration

Henry Law's Constants at temperature 25^oC = 756.7 atm/(mol/litre)
Molar mass of oxygen = 31.9989 g/mol
Mole fraction of oxygen in air = 0.21

Saturation oxygen concentration in water at pressure 1 atm can be calculated as:

C_L^* = [1 (atm) x 0.21 x 31.9989 (g/mol)] / 756.7 (atm/mol.litre)
= 0.0089 g/litre

Appendix C

The specification of boundary conditions

C.1 Simulation of 2 L bioreactor

Table C.1 Rotating domain setting for Impeller1 and Impeller2

Tab	Setting	Value
Basic Settings	Location and Type > Location	Impeller1, Impeller2
	Fluid and Particle Definitions	air
	Fluid and Particle Definitions > air > Material	air at 25 C
	Fluid and Particle Definitions > air > Morphology > Option	Polydispersed Fluid
	Fluid and Particle Definitions	Water
	Fluid and Particle Definitions > air > Material	Fermentation broth
	Fluid and Particle Definitions > air > Morphology > Option	Continuous Fluid
	Domain Models > Pressure > Reference Pressure	
	Domain Models > Buoyancy > Option	
	Domain Models > Buoyancy > Gravity X Dirn	0 [m s^-2]
	Domain Models > Buoyancy > Gravity Y Dirn	-9.81 [m s^-2]
	Domain Models > Buoyancy > Gravity Z Dirn	0 [m s^-2]
	Domain Models > Buoyancy > Buoy.Ref.Density	1000.5 [kg m^-3]
	Domain Models > Buoyancy > Ref Location > Option	Automatic
	Domain Models > Domain Motion > Option	Rotating
	Domain Models > Domain Motion > Angular Velocity	700 [rev min^-1]
	Domain Models > Domain Motion > Axis Definition > Rotation Axis	Global Y
Fluid Models	Multiphase > Homogeneous Model	(Cleared)
	Multiphase > Free Surface Model > Option	None
	Heat Transfer > Homogeneous Model	(Cleared)
	Heat Transfer > Option	Isothermal
	Heat Transfer > Fluid Temperature	25 [C]
	Turbulence > Homogeneous Model	(Cleared)
	Turbulence > Option	Fluid Dependent
	Additional Variable Models > Additional Variable	DO
	Additional Variable Models > DO > Option	Fluid Dependent

Table C.1 Rotating domain setting for Impeller1 and Impeller2 (continued)

Tab	Setting	Value
Poly-dispersed Fluid	Polydispersed Fluid	Polydispersed Fluid 1
	Polydispersed Fluid 1 > Option	Homogeneous MUSIG
	Polydispersed Fluid 1 > Polydispersed Fluid	air
	Polydispersed Fluid 1 > Size Group Distribution > Option	Equal Diameter
	Polydispersed Fluid 1 > Size Group Distribution > Num. Size Groups	10
	Polydispersed Fluid 1 > Size Group Distribution > Minimum Diameter	0.5 [mm]
	Polydispersed Fluid 1 > Size Group Distribution > Maximum Diameter	10 [mm]
	Polydispersed Fluid 1 > Breakup Model	Luo and Svendsen
	Polydispersed Fluid 1 > Coalescence Model	Prince and Blanch
Fluid Specific Models	Fluid	Water
	Fluid > Water > Fluid Buoyancy Model > Option	Density Difference
	Fluid > Water > Turbulence > Option	k-Epsilon
	Fluid > Water > Turbulence > Wall Function	Scalable
	Fluid > Water > Additional Variable Models	DO
	Fluid > Water > Additional Variable Models > DO > Option	Transport Equation
	Fluid	air
	Fluid > air > Fluid Buoyancy Model > Option	Density Difference
	Fluid > air > Turbulence > Option	Dispersed Phase Zero Equation
Fluid Pair Models	Fluid Pair	air | Water
	Fluid Pair > air | Water > Surface Tension Coefficient	(Selected)
	Fluid Pair > air | Water > Surface Tension Coefficient > Surf. Tension Coeff.	0.073 [N m^-1]
	Fluid Pair > air | Water > Momentum Transfer > Drag Force > Option	Grace
	Fluid Pair > air | Water > Momentum Transfer > Drag Force > Volume Fraction Correction Exponent	(Selected)
	Fluid Pair > air | Water > Momentum Transfer > Drag Force > Volume Fraction Correction Exponent > Value	4
	Fluid Pair > air | Water > Momentum Transfer > Non-Drag Forces > Turbulent Dispersion Force > Option	Lopez de Bertodano
	Fluid Pair > air | Water > Momentum Transfer > Non-Drag Forces > Turbulent Dispersion Force > Dispersion Coeff.	0.1

Table C.2 Stationary domain setting for Tank Stationary domain for main tank can be created by copying the properties of the existing impeller domain.

Tab	Setting	Value
Basic settings	Location and Type > Location	Tank
	Domain Models > Domain Motion > Option	Stationary

Table C.3 Boundary condition setting for air inlet

Tab	Setting	Value
Basic settings	Boundary Type	Inlet
	Location	Airinlet
Boundary Details	Mass and Momentum > Option	Fluid Dependent
	Additional Variables > DO > Option	Value
	Add. Var. Value	0.0089 [kg m^-3]
Fluid Values	Boundary Conditions	air
	Boundary Conditions > air > Velocity > Option	Normal Speed
	Boundary Conditions > air > Velocity > Normal Speed	18.1891 [m s^-1]
	Boundary Conditions > air > Volume Fraction > Option	Value
	Boundary Conditions > air > Volume Fraction > Volume Fraction	Water
	Boundary Conditions > Water > Velocity > Option	Normal Speed
	Boundary Conditions > Water > Velocity > Normal Speed	18.1891 [m s^-1]
	Boundary Conditions > Water > Volume Fraction > Option	Value
	Boundary Conditions > Water > Volume Fraction > Volume Fraction	0

Table C.4 Boundary condition setting for outlet

Tab	Setting	Value
Basic Settings	Boundary Type	Oulet
	Location	WALL_LIQUID_SURFACE
Boundary Details	Mass And Momentum > Option	Degassing Condition

Table C.5 Boundary condition setting for Tank shaft

Tab	Setting	Value
Basic Settings	Boundary Type	Wall
	Location	WALL_SHAFT
Boundary Details	Mass and Momentum > Option	Fluid Dependent
	Wall Contact Model > Option	Use Volume Fraction
Fluid Values	Boundary Conditions	air, Water
	Boundary Conditions > air > Mass And Momentum > Option	No Slip Wall
	Boundary Conditions > air > Mass And Momentum > Wall Velocity	(Selected)
	Boundary Conditions > air > Mass And Momentum > Wall Velocity > Option	Rotating Wall
	Boundary Conditions > air > Mass And Momentum > Wall Velocity > Angular Velocity	700 [rev min^-1]
	Boundary Conditions > air > Mass And Momentum > Wall Velocity > Axis Definition > Option	Coordinate Axis
	Boundary Conditions > air > Mass And Momentum > Wall Velocity > Axis Definition > Rotation Axis	Global Y

Table C.6 Boundary condition setting for Tank wall

Tab	Setting	Value
Basic Settings	Boundary Type	Wall
	Location	Wall
Boundary Details	Wall Influence On Flow > Option	No Slip
	Wall Roughness > Option	Smooth Wall
	Wall Contact Model > Option	Use Volume Fraction

Table C.7 Rotational periodic interfaces setting for Impeller 1

Tab	Setting	Value
Basic Setting	Interface Type	Fluid Fluid
	Interface Side 1 > Domian (Filter)	Impeller1
	Interface Side 1 > Region List	Periodic 1.1
	Interface Side 2 > Domian (Filter)	Impeller1
	Interface Side 2 > Region List	Periodic 1.2
	Interface Models > Option	Rotational Periodicity
	Interface Models > Axis Definition > Option	Coordinate Axis
	Interface Models > Axis Definition > Rotation Axis	Global Y
	Mesh Connection Method > Mesh Connection > Option	Automatic

Table C.8 Rotational periodic interfaces setting for Impeller 2

Tab	Setting	Value
Basic Setting	Interface Type	Fluid Fluid
	Interface Side 1 > Domain (Filter)	Impeller2
	Interface Side 1 > Region List	Periodic 2.1
	Interface Side 2 > Domain (Filter)	Impeller2
	Interface Side 2 > Region List	Periodic 2.2
	Interface Models > Option	Rotational Periodicity
	Interface Models > Axis Definition > Option	Coordinate Axis
	Interface Models > Axis Definition > Rotation Axis	Global Y
	Mesh Connection Method > Mesh Connection > Option	Automatic

Table C.9 Rotational periodic interfaces setting for Tank

Tab	Setting	Value
Basic Setting	Interface Type	Fluid Fluid
	Interface Side 1 > Domain (Filter)	Tank
	Interface Side 1 > Region List	Tank_per1
	Interface Side 2 > Domain (Filter)	Tank
	Interface Side 2 > Region List	Tank_per2
	Interface Models > Option	Rotational Periodicity
	Interface Models > Axis Definition > Option	Coordinate Axis
	Interface Models > Axis Definition > Rotation Axis	Global Y
	Mesh Connection Method > Mesh Connection > Option	Automatic

Table C.10 Frozen rotor interfaces setting between Tank and Impeller1
(a) Top interface

Tab	Setting	Value
Basic Settings	Interface Type	Fluid Fluid
	Interface Side 1 > Domain (Filter)	Impeller1
	Interface Side 1 > Region List	TOP1
	Interface Side 2 > Domain (Filter)	Tank
	Interface Side 2 > Region List	BLKBY_TANK_TOP1
	Interface Models > Option	General Connection
	Interface Models > Frame Change/Mixing Model > Option	Frozen Rotor

Table C.10 Frozen rotor interfaces setting between Tank and Impeller1 (continued)
(b) Bottom interface

Tab	Setting	Value
Basic Settings	Interface Type	Fluid Fluid
	Interface Side 1 > Domain (Filter)	Impeller1
	Interface Side 1 > Region List	BOTTOM1
	Interface Side 2 > Domain (Filter)	Tank
	Interface Side 2 > Region List	BLKBY_TANK_ BOTTOM1
	Interface Models > Option	General Connection
	Interface Models > Frame Change/Mixing Model > Option	Frozen Rotor

(c) Outer interface

Tab	Setting	Value
Basic Settings	Interface Type	Fluid Fluid
	Interface Side 1 > Domain (Filter)	Impeller1
	Interface Side 1 > Region List	OUTER1
	Interface Side 2 > Domain (Filter)	Tank
	Interface Side 2 > Region List	BLKBY_TANK_ OUTER1
	Interface Models > Option	General Connection
	Interface Models > Frame Change/Mixing Model > Option	Frozen Rotor

Table C.11 Frozen rotor interfaces setting between Tank and Impeller2
(a) Top interface

Tab	Setting	Value
Basic Settings	Interface Type	Fluid Fluid
	Interface Side 1 > Domain (Filter)	Impeller2
	Interface Side 1 > Region List	TOP2
	Interface Side 2 > Domain (Filter)	Tank
	Interface Side 2 > Region List	BLKBY_TANK_ TOP2
	Interface Models > Option	General Connection
	Interface Models > Frame Change/Mixing Model > Option	Frozen Rotor

Table C.11 Frozen rotor interfaces setting between Tank and Impeller2 (continued)
(b) Bottom interface

Tab	Setting	Value
Basic Settings	Interface Type	Fluid Fluid
	Interface Side 1 > Domain (Filter)	Impeller2
	Interface Side 1 > Region List	BOTTOM2
	Interface Side 2 > Domain (Filter)	Tank
	Interface Side 2 > Region List	BLKBY_TANK_ BOTTOM2
	Interface Models > Option	General Connection
	Interface Models > Frame Change/Mixing Model > Option	Frozen Rotor

(c) Outer interface

Tab	Setting	Value
Basic Settings	Interface Type	Fluid Fluid
	Interface Side 1 > Domain (Filter)	Impeller2
	Interface Side 1 > Region List	OUTER2
	Interface Side 2 > Domain (Filter)	Tank
	Interface Side 2 > Region List	BLKBY_TANK_ OUTER2
	Interface Models > Option	General Connection
	Interface Models > Frame Change/Mixing Model > Option	Frozen Rotor

Table C.12 Solver control setting

Tab	Setting	Value
Basic Settings	Advection Scheme > Option	High Resolution
	Convergence Control > Max. Iterations	3000
	Convergence Control > Fluid Timescale Control > Timescale Control	Physical Timescale
	Convergence Control > Fluid Timescale Control > Physical Control	0.01 [s]
Equation Class Settings	Equation Class	Additional Variable
	Equation Class > Additional Variable > Convergence Control > Time scale Control	Physical Timescale
	Equation Class > Additional Variable > Convergence Control > Physical Timescale	1 [s]

Table C.13 Global Initialization setting

Tab	Setting	Value
Fluid Settings	Fluid Specific Initialization	air
	Fluid Specific Initialization > air > Initial Conditions > Velocity Type	Cartesian
	Fluid Specific Initialization > air > Initial Conditions > Cartesian Velocity Components > Option	Automatic with Value
	Fluid Specific Initialization > air > Initial Conditions > Cartesian Velocity Components > U,V,W	0 [m s^-1]
	Fluid Specific Initialization > air > Initial Conditions > Volume Fraction > Option	Automatic with Value
	Fluid Specific Initialization > air > Initial Conditions > Volume Fraction > Volume Fraction	0.05
	Fluid Specific Initialization	Water
	Fluid Specific Initialization > Water > Initial Conditions > Velocity Type	Cartesian
	Fluid Specific Initialization > Water > Initial Conditions > Cartesian Velocity Components > Option	Automatic with Value
	Fluid Specific Initialization > Water > Initial Conditions > Cartesian Velocity Components > U,V,W	0 [m s^-1]
	Fluid Specific Initialization > Water> Initial Conditions > Volume Fraction > Option	Automatic with Value
	Fluid Specific Initialization > Water > Initial Conditions > Volume Fraction > Volume Fraction	0.95
	Fluid Specific Initialization > Water > Initial Conditions > Additional Variable Details > DO > Option	Automatic with Value
	Fluid Specific Initialization > Water > Initial Conditions > Additional Variable Details > DO > Add. Var. Value	0.0089 [kg m^-3]

Table C.14 Subdomain setting

Tab	Setting	Value
Basic Settings	Location	Tank, Impeller1, Impeller2
Source	Bulk Sources	(Selected)
	Bulk Sources > DO	(Selected)
	Bulk Sources > DO > Option	Source
	Bulk Sources > DO > Option > Source (For Impeller1 and Impeller2)	OTR-OUR
	Bulk Sources > DO > Option > Source (For Tank)	OTRA-OUR
	Bulk Sources > DO > Option > Source > Souce coefficient	1e-10 [s^-1]

Table C.15 Additional Variable setting

Tab	Setting	Value
Basic Settings	Variable Type	Volumetric
	Units	[kg m^-3]
	Tensor Type	Scalar

Table C.16 CEL Expression

Variable	Definition
Tank DO	volumeAve(Water.DO)@Tank
Impeller1 DO	volumeAve(Water.DO)@Impeller1
Impeller2 DO	volumeAve(Water.DO)@Impeller 2
Average DO	(volume()@Tank*Tank DO+volume()@Impeller1*Impeller1 DO+volume()@Impeller 2*Impeller2 DO)/(volume()@Tank+volume()@Impeller1+volume()@Impeller 2)
Im1airholdup	volumeAve(air.Volume Fraction)@Impeller1
Im2airholdup	volumeAve(air.Volume Fraction)@Impeller 2
Tankairholdup	volumeAve(air.Volume Fraction)@Tank
Totalairholdup	(volume()@Tank*Tankairholdup+volume()@Impeller1*Im1airholdup+volume()@Impeller 2*Im2airholdup)/(volume()@Tank+volume()@Impeller1+volume()@Impeller 2)
Masscoeff	0.4*sqrt(2.2875e-9 [m^2 s^-1]*1000.5[kg m^-3]/0.001543[kg m^-1 s^-1])*((Water.Turbulence Eddy Dissipation * 0.001543[kg m^-1 s^-1]/1000.5[kg m^-3])^0.25)
Masscoeff1	2*sqrt(2.2875e-9 [m^2 s^-1]/pi)*((Water.Turbulence Eddy Dissipation * 1000.5[kg m^-3]/0.001543[kg m^-1 s^-1])^0.25)
KLA	Masscoeff*Water | air.Interfacial Area Density
KLA1	Masscoeff1*Water | air.Interfacial Area Density
Dosat	8.9 [g m^-3 Pa^-1] * ((Total Pressure in Stn Frame+ 101325[Pa]) / 101325)
Dosata	8.9 [g m^-3 Pa^-1] * ((Total Pressure + 101325[Pa]) / 101325)
OTR	(Dosat-Water.DO)*Masscoeff*Water | air.Interfacial Area Density
OTRA	(Dosata-Water.DO)*Masscoeff*Water | air.Interfacial Area Density
OUR	2.357e-4[kg m^-3 s^-1]
Totalkla	(volume()@Tank*volumeAve(KLA)@Tank+volume()@Impeller1*volumeAve(KLA)@Impeller1+volume()@Impeller 2*volumeAve(KLA)@Impeller 2)/(volume()@Tank+volume()@Impeller1+volume()@Impeller 2)
Totalkla1	(volume()@Tank*volumeAve(KLA1)@Tank+volume()@Impeller1*volumeAve(KLA1)@Impeller1+volume()@Impeller 2*volumeAve(KLA1)@Impeller 2)/(volume()@Tank+volume()@Impeller1+volume()@Impeller 2)

Appendix D

Ansys CFX Parametric study function

D.1 Working with parameter

Parameter is the feature of ANSYS Workbench. This function enables user to modify the boundary condition of the project so that user can determine the influenced of selected design parameter on the output parameter or the result from simulation without making a new run. For this function, user needs to define the input parameters in CFX pre and output parameter in CFX post. For example, in this work, the effect of agitation speed and air feed rate on the mass transfer coefficient need to be investigated. Therefore, the impeller speed and air feed rate was defined as an input parameter and mass transfer coefficient was defined as an output parameter. The example of input parameter and output parameter was shown in Figure D.1

Outline of Schematic H5: Parameters

	A	B	C	D
1	ID	Parameter Name	Value	Unit
2	Input Parameters			
3	CFX (H1)			
4	P6	airinlet	20.723	m s^-1
5	P7	Imspeed	400	rev min^-1
*	New input parameter	New name	New expression	
7	Output Parameters			
8	CFX (H1)			
9	P5	Totalkla	0.030238	s^-1
*	New output parameter		New expression	
11	Charts			
12	Parameter Chart 0			

Figure D.1 Outline of input parameter and output parameter

After the defining the input parameter and output parameter step, user can manually change the values of input parameter to the effect on the output parameter. The example was shown in Figure D.2. User can specific the air inlet value and agitation speed value in the row B and row C, respectively. The simulation will run automatically and the results will be shown in row D.

Table of Design Points

	A	B	C	D	E	F
1	Name	P6 - airinlet	P7 - Imspeed	P5 - Totalkla	Exported	Note
2		m s^-1	rev min^-1	s^-1		
3	Current	20.723	400	0.030238		0.5 vvm
4	DP 1	20.723	450	0.037271	☑	0.5 vvm
5	DP 2	20.723	500	0.052872	☑	0.5 vvm
6	DP 3	20.723	550	0.078849	☑	0.5 vvm
7	DP 4	20.773	600	0.10734	☑	0.5 vvm
*					☐	

Figure D.2 Table of design point

D.1.1 Using parameter function to investigate the effect of air feed rate on mass transfer coefficient of 200 L bioreactor scale

Operating agitation speed: 480 rpm and 600 rpm
Operating air feed rate : 0.1, 0.15, 0.3, 0.5, 0.7 and 1vvm

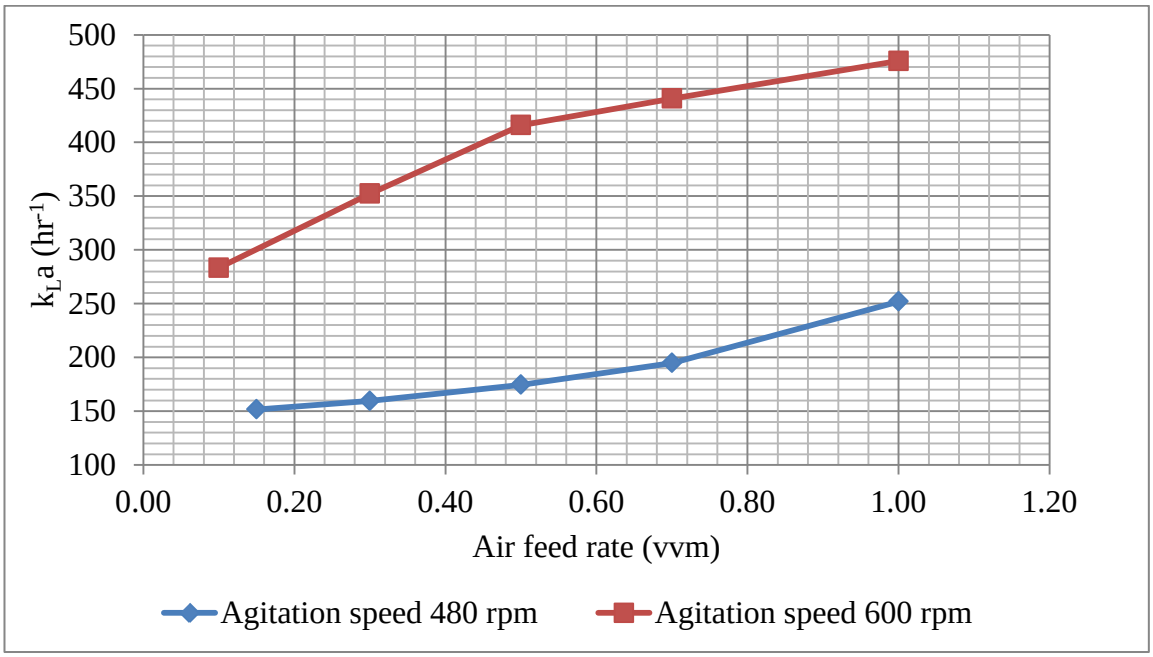

Figure D.3 The effect of air feed rate on mass transfer coefficient

D.1.2 Using parameter function to investigate the effect of agitation speed on mass transfer coefficient of 200 L bioreactor scale

Operating agitation speed: 400, 450, 500, 550, 600 rpm
Operating air feed rate : 0.5 vvm

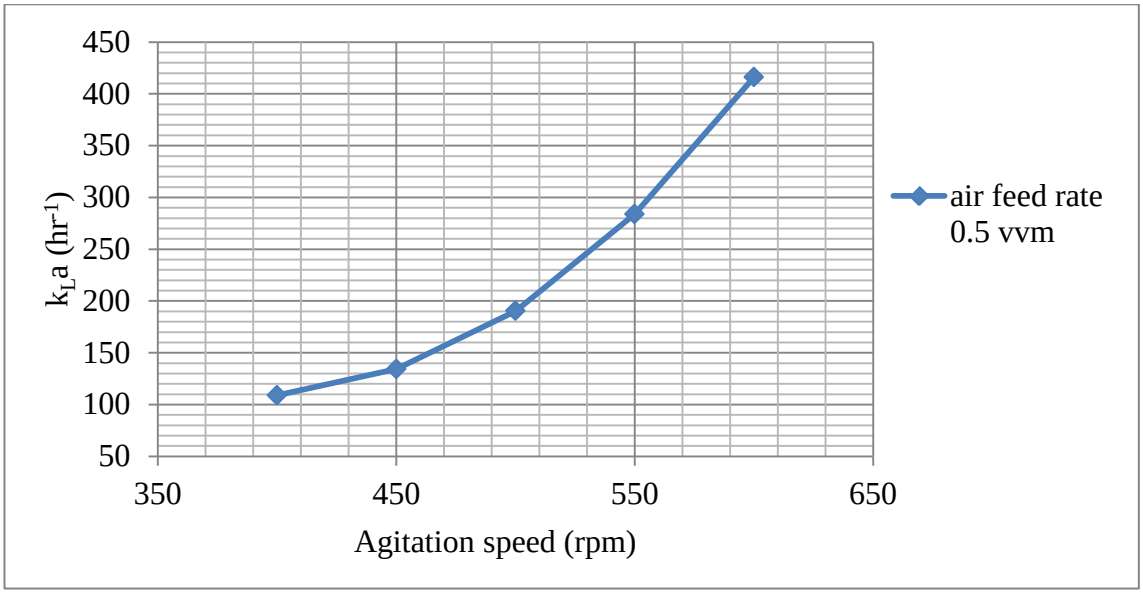

Figure D.4 The effect of agitation speed on mass transfer coefficient

CURRICULUM VITAE

NAME	Mr. Pisut Veerahong
DATE OF BIRTH	13 May 1988
EDUCATIONAL RECORD	
HIGH SCHOOL	High School Graduation Wat Rajadhivas School, Bangkok, 2005
BACHELOR'S DEGREE	Bachelor of Engineering (Chemical Engineering) King Mongkut's University of Technology Thonburi, 2009
MASTER'S DEGREE	Master of Engineering (Chemical Engineering) King Mongkut's University of Technology Thonburi, 2011